Calpastatin prevents Angiotensin II–mediated podocyte injury through maintenance of autophagy

Imane Bensaada, Blaise Robin, Joëlle Perez, Yann Salemkour, Anna Chipont, Marine Camus, Mathilde Lemoine, Lea Guyonnet, Hélène Lazareth, Emmanuel Letavernier, et al.

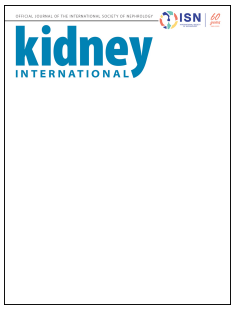

Calpastatin prevents Angiotensin II-mediated podocyte injury through maintenance of autophagy

Imane Bensaada, PhD, Blaise Robin, MS, Joëlle Perez, MS, Yann Salemkour, MS, Anna Chipont, BS, Marine Camus, BS, Mathilde Lemoine, MD, Lea Guyonnet, PhD, Hélène Lazareth, Emmanuel Letavernier, MD, PhD, Carole Hénique, PhD, Pierre-Louis Tharaux, MD, PhD, Olivia Lenoir, PhD

PII: S0085-2538(21)00266-0

DOI: https://doi.org/10.1016/j.kint.2021.02.024

Reference: KINT 2512

To appear in: *Kidney International*

Received Date: 5 August 2020

Revised Date: 29 January 2021

Accepted Date: 10 February 2021

Please cite this article as: Bensaada I, Robin B, Perez J, Salemkour Y, Chipont A, Camus M, Lemoine M, Guyonnet L, Lazareth H, Letavernier E, Hénique C, Tharaux PL, Lenoir O, Calpastatin prevents Angiotensin II-mediated podocyte injury through maintenance of autophagy, *Kidney International* (2021), doi: https://doi.org/10.1016/j.kint.2021.02.024.

Calpastatin prevents Angiotensin II-mediated podocyte injury through maintenance of autophagy

Wild-type

+ Angiotensin II
+ 3% NaCl Food

P62/PODXL

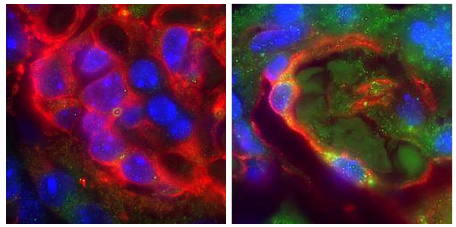

Baseline Hypertension

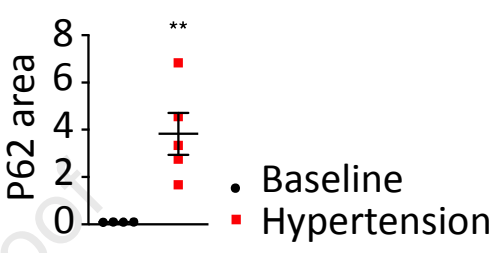

AngII-mediated autophagy blockade

ATG5$^{\Delta podocyte}$

+ Angiotensin II
+ 3% NaCl Food

NPHS1/WT1

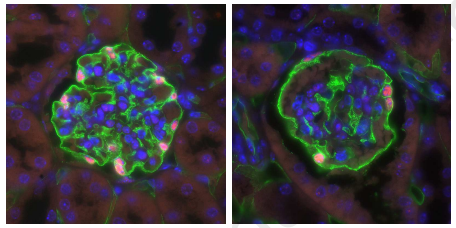

Wild-type ATG5$^{\Delta podocyte}$

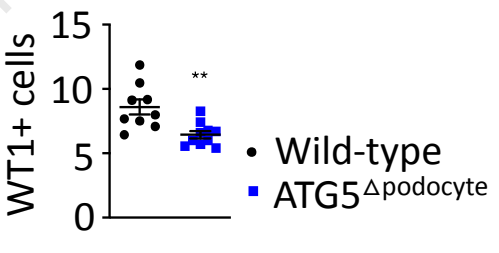

Autophagy deficiency promotes AngII-mediated podocyte injury

Calpastatin^{Tg}

+ Angiotensin II
+ 3% NaCl Food

P62/PODXL

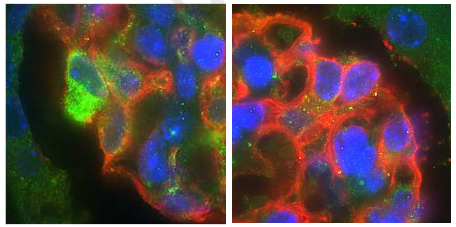

Wild-type Calpastatin^{Tg}

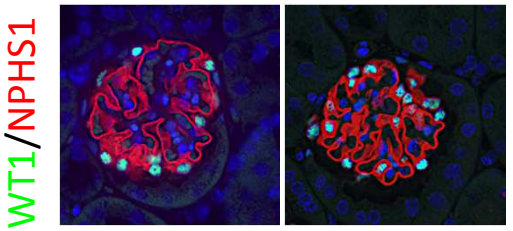

Wild-type Calpastatin^{Tg}

Calpastatin prevents AngII-mediated autophagy blockade and podocyte injury

CONCLUSION:
Calpastatin overexpression prevents angiotensin II-mediated podocyte injury through maintenance of autophagy

kidney INTERNATIONAL
OFFICIAL JOURNAL OF THE INTERNATIONAL SOCIETY OF NEPHROLOGY

Bensaada, Robin et al. 2020

[QUERY TO AUTHOR: title and abstract rewritten by Editorial Office – not subject to change]

Calpastatin prevents Angiotensin II-mediated podocyte injury through maintenance of autophagy

Running title: AngII-modulated autophagy in hypertensive nephropathy

Imane Bensaada, PhD [1,#], Blaise Robin, MS [1,#], Joëlle Perez, MS [2], Yann Salemkour, MS [1], Anna Chipont, BS [1], Marine Camus, BS [1], Mathilde Lemoine, MD [1], Lea Guyonnet, PhD [1], Hélène Lazareth [1], Emmanuel Letavernier, MD, PhD [2], Carole Hénique, PhD [1], Pierre-Louis Tharaux, MD, PhD [1,*] and Olivia Lenoir, PhD [1,*]

[1] Université de Paris, PARCC, Inserm, F-75015Paris, France.

[2] Université Paris Descartes, Sorbonne Paris Cité, Paris, France.

[#] equal contribution

[*] corresponding authors

Correspondence: Olivia Lenoir, PhD or Pierre-Louis Tharaux, MD, PhD.

Paris Cardiovascular Research Center 56 rue Leblanc 75015 PARIS, France

Cell: +33 1 53 98 80 19 - Fax : +33 1 53 98 79 53

E-mail : olivia.lenoir@inserm.fr or pierre-louis.tharaux@inserm.fr

Fundings to acknowledge:

O.L.: European Foundation for the Study of Diabetes (EFSD), Société Francophone du Diabète (SFD); B.R., C.H., P-L.T.: European Research Council; I.B: French Ministry of Research; Y.S.: Fondation de France; Inserm Institut National de la Santé Et de la Recherche Médicale and Université de Paris

ABSTRACT

The strong predictive value of proteinuria in chronic glomerulopathies is firmly established as well as the pathogenic role of angiotensin II promoting progression of glomerular disease with an altered glomerular filtration barrier, podocyte injury and scarring of glomeruli. Here we found that chronic angiotensin II-induced hypertension inhibited autophagy flux in mouse glomeruli. Deletion of *Atg5* (a gene encoding a protein involved autophagy) specifically in the podocyte resulted in accelerated angiotensin II-induced podocytopathy, accentuated albuminuria and glomerulosclerosis. This indicates that autophagy is a key protective mechanism in the podocyte in this condition. Angiotensin-II induced calpain activity in podocytes inhibits autophagy flux. Podocytes from mice with transgenic expression of the endogenous calpain inhibitor calpastatin displayed higher podocyte autophagy at baseline that was resistant to angiotensin II-dependent inhibition. Also, sustained autophagy with calpastatin limited podocyte damage and albuminuria. These findings suggest that hypertension has pathogenic effects on the glomerular structure and function, in part through activation of calpains leading to blockade of podocyte autophagy. These findings uncover an original mechanism whereby angiotensin II-mediated hypertension inhibits autophagy via calcium-induced recruitment of calpain with pathogenic consequences in case of imbalance by calpastatin activity. Thus, preventing a calpain-mediated decrease in autophagy may be a promising new therapeutic strategy for nephropathies associated with high renin- angiotensin system activity.

Keywords: Angiotensin II, autophagy, podocyte, calpastatin, hypertension.

TRANSLATIONAL STATEMENT

Given the crucial role of autophagy in the development of kidney diseases, pharmacological modulation of autophagy might be a promising strategy for the prevention and treatment of several renal diseases. In parallel, overactivation of calpain activity in podocytes was found to play detrimental effects on podocyte function whereas its deleterious mechanisms of action were not identified. Here, we provide evidence that calpain links the deleterious action of angiotensin II to the detrimental blockade of autophagy in podocyte and suggest that calpain inhibition could be a promising therapeutic target for podocyte diseases partially through maintenance of podocyte autophagy.

INTRODUCTION

Hypertension is second only to diabetes as a leading cause of progressive chronic kidney disease[1-3] and even modest elevation in blood pressure is an independent risk factor for end-stage kidney disease[4]. An increasing number of experimental studies have highlighted the importance of podocyte in the development of kidney injury. Progressive loss of podocytes and microvascular alterations appear early with the functional renal decline in experimental hypertensive nephropathy[5]. In patients, urinary excretion of viable podocytes was shown to be a sensitive and specific marker for preeclampsia[6, 7] and patients with nephrosclerosis had a significantly lower density of glomerular podocytes than did kidney donors[8, 9]. Furthermore, the pathogenic role of angiotensin II (AngII) promoting progression of glomerular disease is well established, not only in hypertensive conditions but also in several glomerular diseases[10-21].

Glomerular hypertension results in glomerular capillary stretching, endothelial damage and elevated glomerular protein filtration causing glomerular collapse and glomerulosclerosis. It also exerts a direct action on glomerular structures, causing signaling regulatory responses aimed to compensate. Activated systemic and local renin-angiotensin-aldosterone system (RAAS), fosters mesangial hyperplasia and synthesis of vascular permeability factors. Concomitantly, podocytes display calcium

signaling[22, 23] and modify their shape upon AngII type 1 receptor (AT1) dependent stimulation[24-28]. These adaptive mechanisms become maladaptive in the long term, finally leading to glomerulosclerosis. AT1 mediates prominent RAAS involvement for blood pressure and salt and water homeostasis. Angiotensin-converting enzyme inhibitors (ACEI) and AT1 blockers are clinically used for the treatment of hypertension and heart failure in patients. Interestingly, both blockers also show a protective effect on kidney function.

Autophagy was demonstrated to be essential for the maintenance of cellular homeostasis, particularly in post-mitotic cells[29, 30], and notably podocytes[31-34]. Autophagy is a lysosomal-associated degradation system for long-lived cytoplasmic proteins and dysfunctional organelles[35, 36] and involves sequestration of proteins and organelles in autophagosomes. The formation of autophagosomes is dependent on the induction of several genes including *Map1lc3a/b*, *Beclin 1*, and *Atgs*[37]. There is growing evidence that dysregulation of the autophagic pathway is implicated in the pathogenesis of kidney aging and several renal diseases such as acute kidney injury (AKI), polycystic kidney disease (PKD), aging, and diabetic nephropathy (DN)[31, 32, 38-41].

Regulation of autophagy in podocytes, in physiological, and above all, in pathological context, is not well known. We recently demonstrated that podocyte autophagy is independent of mTOR regulation in physiological condition, making this cell type an exception[42]. AT1 activation stimulates protein synthesis and protein turnover in cells. Thus, we reasoned that activation of the RAAS may also influence protein turnover stimulation and proteostasis.

In the present study we focused on the role of AngII signaling in podocyte autophagy regulation. We identified the calcium-activated proteases calpains mediating a chronic blocking effect of AngII on podocyte autophagy. Further, we found that the endogenous calpain inhibitor calpastatin was able to prevent AngII-dependent autophagy inhibition and podocyte injury during hypertension.

These findings uncover an original mechanism whereby AngII-mediated hypertension inhibits autophagy *via* calcium-induced recruitment of calpain with pathogenic consequences in case of imbalance by calpastatin activity.

METHODS

Animals

Calpastatin-Tg mice were kindly provided by Dr E. Letavernier[43]. Mice with a podocyte-specific disruption of the *Atg5* gene (*Nphs2*.cre *Atg5*$^{lox/lox}$), generated as previously described[31] by crossing *Nphs2*.Cre mice[44] with *Atg5*$^{lox/lox}$ mice[45] on C57BL6/J background. *Nphs2*.cre *Atg5*$^{lox/lox}$ mice and control littermates males, aged 10–12 weeks, were used in this study. Hypertensive model was induced by subcutaneous infusion of AngII (Sigma-Aldrich, A9525) at a dose of 1 µg/kg/min for 4 to 6 weeks *via* osmotic minipumps (Alzet Corp, Model 2006). Pumps were implanted subcutaneously on the back between the shoulder blades and hips. Mice received salt supplementation (3% NaCl) in food. *Atg5*$^{lox/lox}$ (wild type, WT) mice were used as controls in all studies. For DOCA-salt with nephron reduction model, adult male underwent unilateral left nephrectomy. 2 weeks after nephrectomy, they received deoxycorticosterone acetate (DOCA) pellets with 21-day release (Innovative Research of America) implanted sub-cutaneously. A second pellet was implanted 3 weeks after the first implant. All mice received 0,9% NaCl in drinking water ad libitum and were sacrified after 6 weeks of DOCA administration[46]. Experiments were conducted according to the French veterinary guidelines and those formulated by the European Community for experimental animal use (L358-86/609EEC), and were approved by the French Ministry of Research and local University Research Ethics Committee (APAFIS-7646 and -22373).

Primary podocyte culture experiment

Culture of differentiated primary podocytes was performed as previously described[47, 48]. Briefly, freshly isolated renal cortex was mixed and digested by collagenase I (Gibco-17100-017) in RPMI 1640 (Life Technologies, 61870-044). Tissues were then passed through 70 µm and 40 µm cell strainers (BD falcon-352340 and -352350). Glomeruli, which adhere to the 40 µm cell strainer, were removed with phosphate-buffered saline (PBS; Life Technologies, 10010023) + 0.5% BSA (Eurobio-

HALALB07-65) injected under pressure, and were then washed twice in PBS. Freshly isolated glomeruli were plated in 6-well dishes in RPMI 1640 (Gibco-61870036) supplemented with 10% fetal calf serum and 1% penicillin/streptomycin (Life Technologies-15140122) to allow podocytes to exit from glomeruli and grow. Podocyte enrichment was verified by western blot as previously described[31, 48, 49] (**Fig.S1**). Podocytes were cultured in the absence or presence of bafilomycin A1 (100 nmol/L, Sigma-Aldrich-B1793) for 4 hours. For immunofluorescence experiments, primary podocytes were plated on 4 dishes labtek (Dutsher-055071). Podocytes were then fixed in PFA 4% for 10 minutes and processed for immunofluorescence.

Calpain activity assay

Intracellular calpain activity was determined in primary podocytes, as previously described[50-52]. 100 000 cells were cultured in 24-well tissue culture dishes in RPMI 1640 supplemented with 10% fetal calf serum and 1% penicillin/streptomycin. After the indicated culture period, the medium was replaced with KRH solution (pH 7.4) containing 4 mM CaCl2, with or without 10µM calpain inhibitor-1, and incubated for 10 minutes before the addition of 50mM calpain substrate N-succinyl-Leu-Leu-Val-Tyr-7-amino-4-methylcoumarin (Sigma-Aldrich-S6510). After a 90-minute incubation period, calpain activity was determined as the difference between fluorescence (measured at 360 nm excitation and 430 nm emission) with and without calpain inhibitor-1.

Western blot

Primary podocytes were scratched with 80µl of RIPA buffer containing phosphatase and protease inhibitor. Protein concentration was measured with BCA Protein Assay Kit (Merck Biochemistry-71285). Twenty micrograms of proteins were electrophoresed on Criterion TM XT precast gel (12% Bis-tris, Biorad-3450124). The proteins were transferred into polyvinylidene difluoride membrane (Thermofischer scientific-88518). After blocking in 5% milk in TBS-T, membranes were incubated with rabbit polyclonal anti-LC3 (1:1000, cell signaling technology-#2575), rabbit polyclonal anti-ATG5

(1:2000, cell signaling technology-#2630), guinea-pig polyclonal anti-SQSTM1/P62 (1:10000, Progen-GP62), rabbit polyclonal anti-calpain 1 domain IV, (1:1000, Abcam-ab39170), rabbit polyclonal anti-calpain 2 amino-terminal end domain I (1:1000, Abcam -ab 39165) and mouse monoclonal IgG1 anti-Calpain 4 (1:1000, Santa Cruz biotechnology-sc-32325), rabbit anti-podocin (1:1000, Abcam-Ab50339), Guinea-pig anti-nephrin (1:500, Progen-GP-N2), rat monoclonal anti-TUBA/tubulin antibody (1:5000, Abcam-ab6160). After washing, membranes were incubated with horseradish peroxidase linked antibody (1:2000, cell signaling technology-7074,7076,7077). The detection of specific signals was performed using the ECL Chemiluminescent Kit (Biorad-170-5070) on a LAS4000 device (Fuji). Densitometry analysis with Image J software (NIH) was used for quantification.

Blood pressure measurements and physiological assessments

Systolic blood pressure (SBP) of mice was recorded by the tail-cuff method (Visitech Systems Inc., BP-2000). Ten measurements from each mouse were taken and then a mean value was determined. SBP was measured at baseline (12-weeks of age) and then weekly until the end of the treatment period. All mice were placed in metabolic cages with free access to water for 6-hour urine collection. Urinary creatinine and plasma urea concentrations were analyzed spectrophotometrically by a colorimetric method (Olympus, AU400). Urinary albumin excretion was measured using a specific ELISA assay for the quantitative determination of albumin in mouse urine (Crystal chem-80630).

Histology

Kidneys were harvested and fixed in 4% PBS-buffered formalin. Paraffin-embedded sections (3 µm thick) were stained by Masson's trichrome to evaluate kidney morphology. Abnormalities in kidneys were graded based on the presence and severity of component abnormalities, including glomerulosclerosis, mesangial expansion, tubular atrophy or casts and fibrosis. The proportion of sclerotic glomeruli was evaluated by a blind examination of at least 50 glomeruli per kidney section.

Immunofluorescence staining of kidney sections and primary podocytes

Fixed primary podocytes were blocked in TBS-T 3% BSA, and incubated overnight at 4°C with primary antibodies guinea-pig anti-SQSTM1/P62 (1:1000, GP-62C, Progen) and rabbit anti-GFP (1:500, ab290, Abcam). After TBS-T rinses, fluorophore-conjugated secondary antibodies, donkey anti-guinea-pig IgG AF594-conjugated antibody (Jackson ImmunoResearch-706-585-148) and donkey anti-rabbit IgG AF488-conjugated antibody (Invitrogen-A21206), were applied. Images were taken using a Zeiss 2 fluorescent microscope, AxioCam HRC camera and the Axiovision 4.3 software.

For FFPE kidneys, sections (3 µm) were deparaffinized, hydrated and antigen retrieval was performed in heated citrate buffer pH=6. Sections were then permeabilized with Triton 0,1% and blocked in TBS-T 3% BSA before overnight antibody incubation at 4°C. We used a goat anti-NPHS1/Nephrin antibody (1:100, Progen-GP-N2), a guinea-pig anti-SQSTM1/P62 (1:1000, Progen- GP-62C), a rabbit anti-GFP (1:1000, Abcam-ab290), a goat anti-PODXL (1:1000, Bio-techne-AF-1556) and a rabbit anti-WT1 (1:100, Abcam-ab192). Secondary antibodies were Alexa-488 and Alexa-568 conjugated antibodies from Invitrogen. Nuclei were stained in blue using Hoechst. Slides were mounted using fluorescent mounting medium (Dako-S3023). Photomicrographs were taken with an Axiophot Zeiss photomicroscope (Jena) and the Axiovision software. Semi-automatic quantifications on Fiji were used for quantifications of NPHS1+ and PODXL+ areas per glomerular section on at least 30 glomeruli per mouse. Podocyte number was counted as the number of WT1+ nuclei per glomerular section on at least 30 glomeruli per mouse.

Transmission Electron Microscopy Procedure

Small pieces of renal cortex (1 mm^3) were fixed in 3% glutaraldehyde EM grade (Electron Microscopy Science) for 1-to-30 days, and washed 3 times in PBS. Samples were postfixed in 1% osmium tetroxide 0.1M (Electron Microscopy Science) in 0.1 M PBS (pH 7.4) and washed in water. Samples were dehydrated in alcohol grades and 100% Propylene oxide (Electron Microscopy Science). Resin infiltration was performed as following: mix 1:1 Epikote 812: propylene oxide 30 min followed by mix

1:2 Epikote 812: propylene oxide overnight room temperature. Samples were embedded in 4mm gelatin capsules in 100% Epikote 812, and Polymerized in 60ºC oven. Ultrathin sections were cut with a Leica UFC7 ultramicrotome (Leica Microsystems GmbH) and deposed on Gilder grids 200 mesh (Electron Microscopy Science). They were counterstained with uranyl acetate 7% (LFG) and Reynold's lead citrate (LFG). Samples were examined in a JEOL 1011 transmission electron microscope (JEOL) with an ORIUS 1000 CCD camera (GATAN), operated with Digital Micrograph software (GATAN) for acquisition.

qPCR array

Freshly isolated glomeruli were frozen in Qiazol reagentat -80°C. Total RNA extraction using the phenol-based method was processed according to the manufacturer's recommendations. cDNAs were synthetized using the RT^2 first strand kit (Qiagen, 330401) and real-time PCR was performed using Custom RT^2 profiler PCR Array (Qiagen, CLAM36771C) with RT^2 SYBR qPCR Mastermix (Qiagen, 330502). qPCR plates were run on an Applied Biosystems StepOnePlus cycler. Each array contains quality control for reverse transcription efficiency and gDNA contamination. qPCR analysis was done by the 2-DDCT method with help of the GeneGlobe Data Analysis Center (www.qiagen.com/shop/genes-and-pathways/data-analysis-center-overview-page) and expressed as the Log2 fold change in gene expression.

***In silico* proteomic analysis**

In silico prediction of calpain cleavage site was done with DeepCalpainPredict (http://deepcalpain.cancerbio.info/help.php), GPS-CCD (http://ccd.biocuckoo.org) and CaMPDB (http://calpain.org/) online tools. Mouse protein amino acid sequence was obtained from Uniprot (https://www.uniprot.org). Results are resumed in **Table S1** and **File S1.**

Statistical analyses

All graphs represent individual values and means +/-SEM. Statistical analyses were calculated using GraphPad Prism software (La Jolla, CA). Comparison between two groups was performed by a parametric Student t-test when samples passed the Anderson-Darling and D'Agostino normality tests and F test for equality of variance. Otherwise a non-parametric Mann-Whitney test was used. Comparison between multiple groups was performed by one-way or two-way ANOVA followed by multiple comparison test with Sidak's correction. Values of $p<0.05$ were considered significant. * $p<0.05$, ** $p<0.01$, *** $p<0.001$

RESULTS

Angiotensin II + HSD- induced hypertension inhibited podocyte autophagy

Podocytes present a high level of autophagy *in vivo,* as shown by strong GFP expression in transgenic mice with GFP fusion to LC3 (GFP-LC3 mice), a key marker of autophagy (**Fig.S2A**). Autophagy is a dynamic process with constant formation of autophagosome and degradation of the autophagolysosomes. Blocking autophagosomal degradation with chloroquine (CQ) resulted in accumulation of GFP+ dots, indicating high autophagic flux in podocytes (**Fig.S2A,B**). Confirmation that GFP+ dots were autophagosomes was shown by double immunofluorescence for GFP and P62/SQSTM1, a chaperone protein degraded by autophagy (**Fig.S2C,D**). Again, CQ treatment induced accumulation of GFP+ P62+ dots, demonstrating important autophagic flux in podocyte. Finally, high autophagic flux was conserved *in vitro* as shown by GFP and P62 expression in primary podocyte isolated from GFP-LC3 mice and strong accumulation of GFP+ and P62+ dots under Bafilomycin A1 treatment, another blocker of autophagosomal degradation (**Fig.S2E-H**).

The capacity of hypertension to modulate podocyte autophagic responses was then assessed in mice infused with AngII with high salt diet (HSD) for 6 weeks and in non-hypertensive controls. As shown in Figure 1, AngII +HSD induced P62 accumulation in glomeruli with strong accumulation in podocyte, thus suggesting that AngII +HSD was responsible for podocyte autophagy blockade (**Fig.1A-D**). Interestingly, P62 accumulation in podocyte was similar to the one observed in mice deficient for

podocyte autophagy (*Nphs2*-Cre *Atg5*$^{lox/lox}$ mice). In another model of hypertension, the DOCA-salt model, we also observed progressive P62 accumulation in podocytes along the time course of the disease (**Fig.S3**).

Deletion of *Atg5* specifically in podocytes results in increased albuminuria, podocyte loss and glomerular injury in AngII + HSD model

We then examined whether autophagy blockade only in podocytes (*Nphs2*-cre *Atg5*$^{lox/lox}$ mice) affects glomerular injury in AngII + HSD model. We first confirmed that *Nphs2*-cre *Atg5*$^{lox/lox}$ mice had normal blood pressure, normal kidney function and no glomerular histological lesions until 10 months of age, as previously reported (**Fig.S4**)[32]. Then, *Atg5*$^{lox/lox}$ (WT) and *Nphs2*-cre *Atg5*$^{lox/lox}$ mice were infused with AngII with HSD for 6 weeks. Importantly, systolic blood pressure was similar in the two groups after AngII infusion during the course of the study (**Fig.2A**), although the tail-cuff method used to measure blood pressure might not have the ability to resolve small blood pressure differences. AngII infusion with HSD markedly increased urinary albumin-to-creatinine ratio in WT mice, and this effect was further significantly increased in *Nphs2*-cre *Atg5*$^{lox/lox}$ mice (**Fig.2B**). Hypertensive *Nphs2*-cre *Atg5*$^{lox/lox}$ mice also displayed significantly increased glomerular sclerosis when compared to WT littermates (**Fig.2C-E**). In agreement with the measured proteinuria, proteinaceous casts and tubular dilatation were significantly more prevalent in mice with podocyte deficiency in ATG5 (**Fig.2F-H**).

Podocyte number per glomerulus was significantly decreased in *Nphs2*-cre *Atg5*$^{lox/lox}$ mice treated with AngII + HSD (**Fig.2I-K**). Podocyte injury in *Nphs2*-cre *Atg5*$^{lox/lox}$ mice with AngII infusion + HSD even progressed to focal and segmental glomerulosclerosis (FSGS) as shown by expression of the PEC activation marker CD44 in glomeruli (**Fig.2L,M**). Electron microscopy analysis identified significant changes associated with ATG5 deficiency upon chronic AngII infusion with HSD, including foot process effacement in hypertensive *Nphs2*-cre *Atg5*$^{lox/lox}$ mice. By contrast, few ultrastructural defects were found in podocytes from WT mice even after 10 weeks of AngII infusion with HSD

(**Fig.2N,O**); indicating that the autophagic activity of podocytes is required for their resistance to AngII + HSD-induced damage. Altogether, our results indicated that, in AngII + HSD model, autophagy inhibition aggravates podocyte injury and loss and induces subsequent FSGS.

AngII + HSD activates calpain activity in podocyte that contributes to autophagy blockade

As calpain activity was found (1) to be activated by AngII in several cell types and (2) to cleave several autophagy-related proteins[53], we wondered if AngII + HSD-mediated autophagy blockade could be attributable to increased AngII-induced calpain activity. We first found that primary podocytes expressed the three ubiquitous forms of calpains (**Fig.3A**). We then showed that AngII stimulated calpain activity in primary podocytes. This rise in calpain activity was blocked by a selective calpain inhibitor (**Fig.3B**). We used a knock-in mouse with extra calpastatin transgene expression (leading to decreased calpain activity)[43], to assess the role of calpains in AngII + HSD-mediated renal injury and autophagy blockade. Primary podocytes from calpastatin transgenic mice (CST^{Tg}) showed decreased calpain activity in response to AngII when compared to podocytes from control mice (**Fig.3C**). Thus, calpastatin overexpression in podocyte decreased AngII-mediated calpain activation.

We next assessed autophagy levels in podocyte from CST^{Tg} mice. We generated CST^{Tg} mice with GFP-LC3 transgene. LC3-GFP reporter allowed counting of autophagosomes as GFP+/P62+ dots. P62 will accumulate in aggregates in cells when autophagic flux is blocked. At basal state, we counted less GFP+ P62+ dots (**Fig.4A,B,E**) and less P62 accumulation (**Fig.4C,D,F**) in podocytes of the CST^{Tg} GFP-LC3 mice than in podocytes of the normal GFP-LC3 mice, suggesting increased autophagic flux in podocytes of mice with high calpastatin abundance.

Autophagic flux can be monitored by measurement of the conversion of the cytoplasmic form of LC3, LC3-I, to the autophagosomal cleaved and phosphatidyl-ethanolamine (PE)-coupled form of LC3, LC3-II, on Western blot. Podocytes from CST^{Tg} mice showed increased LC3-I to LC3-II conversion and decreased P62 expression, both in presence and absence of Bafilomycin A_1 (**Fig.5A,B**), indicating increased autophagic flux in podocytes with calpastatin overexpression. Finally, accumulation of

GFP+ P62+ dots in podocytes after chloroquine administration was more important in CST^{Tg} GFP-LC3 mice than in GFP-LC3 mice, thus confirming that calpastatin overexpression induces autophagic flux in podocytes *in vivo* (**Fig.5C-E**). Altogether, our data suggest that AngII stimulates calpain activity in podocytes, autophagy is inhibited by calpain in podocytes and that inhibition of the endogenous calpain activity by calpastatin overexpression is sufficient to stimulate autophagic flux in podocytes.

Calpastatin Tg mice are protected from AngII + HSD-induced podocyte injury

CST^{Tg} mice did not show any renal alteration until at least 12 months-old (**Fig.S5**). We analyzed podocyte injury in CST^{Tg} mice during Ang II + HSD treatment. While WT mice developed mild glomerulosclerosis and podocyte injury after four weeks of hypertension, as shown by abnormal expression of podocalyxin and nephrin; CST^{Tg} mice presented less sclerotic glomerular lesions (**Fig.6A-B**) and preserved podocalyxin and nephrin expression (**Fig.6C-H**). Such differences in podocyte phenotype were observed at a stage where the density of podocyte nuclei, was not different between WT and CST^{Tg} hypertensive mice (**Fig.6I-K**).

Similarly, after 6 weeks of hypertension, GFP-LC3 and GFP-LC3 CST^{Tg} mice presented podocyte injury but lesions were more prominent in the GFP-LC3 mice (**Fig.7**). Urine albumin-on-creatinine ratio was higher in GFP-LC3 mice after 4 weeks of AngII + HSD (**Fig.7A**). Podocyte number was not different between the two genotypes but nephrin expression was significantly more decreased in the GFP-LC3 control mice (**Fig.7B-E**). Correlating with CST-mediated protection, ultrastructural analysis mild and focal podocyte foot process effacement in GFP-LC3 mice treated with AngII + HSD with better preservation of the foot process in the CST^{Tg} mice, although the global quantification of the number of foot process per GBM length was not statistically different, most likely because because podocyte injury keeps focal and segmental in our model (**Fig.7F-H**). Of note, macrophages and T lymphocyte infiltration in kidneys were not different between the groups (**Fig.S6**). Taken together these results demonstrated that calpastatin prevented AngII + HSD-induced podocyte injury.

Calpastatin overexpression restores autophagic flux in podocyte in mice after AngII + HSD treatment

Finally, we wondered if calpastatin-mediated glomerular protection in the AngII + HSD model implicated autophagy maintenance in podocyte. Interestingly, AngII + HSD-induced P62 accumulation in podocyte was prevented in CST^{Tg} and GFP-LC3 CST^{Tg} mice (**Fig.8A-D**), indicating that calpastatin prevented blockade of podocyte autophagy. To note, the number of GFP+ P62+ dots labeling of autophagosomes, were similar in podocyte from hypertensive GFP-LC3 and GFP-LC3 CST^{Tg} mice, thus suggesting that AngII + HSD induced a slowdown of the podocyte autophagic flux rather than a complete arrest (**Fig.8E-G**).

***In silico* prediction of calpain cleavage site in podocyte proteins**

We used several *in silico* tools to predict potential calpain targets in podocyte (**Table S1 and File S1**). Three online database were compared: GPS-CCD[54], CaMPDB[55] and DeepCalpain[56]. *In silico* analysis identified several podocyte proteins, nephrin and podocin among them, that could be cleaved by calpains. Thus, calpastatin-mediated glomerular protection could be linked to a reduction of calpain enzymatic activity leading to reduced degradation of some podocyte protein.

Furthermore, at least three autophagy-related proteins are direct targets of calpains. ATG5 is cleaved by calpains, leading to a disturbance of the ATG12-ATG5 complex formation[57, 58]. Administration of calpain inhibitors *in vivo* also prevented cleavage of the autophagy protein beclin-1[59]. *In silico* analysis of putative cleavage site on autophagy-related proteins support the hypothesis that calpain could regulate autophagy through enzymatic cleavage of autophagy proteins.

mRNA expression of ER and oxidative stress markers in glomeruli from mice treated with AngII + HSD.

We evaluated ER stress and oxidative stress by qPCR in glomeruli during AngII + HSD treatment. At

baseline, we did not observe any change in mRNA expression of analyzed genes in glomeruli from WT and *Nphs2*.cre *Atg5*$^{lox/lox}$ mice (**Fig.S7**). After 6 weeks of hypertension, glomeruli from *Nphs2*.cre *Atg5*$^{lox/lox}$ mice showed different mRNA profile of genes of the ER stress and oxidative stress pathways with increased expression of *Sod1*, *Prdx1*, *Atf4*, *Gpx1* and *Hsp90b1* as compared to WT glomeruli, thus suggesting that autophagy depletion in podocyte favoured AngII + HSD-induced ER stress and oxidative stress. Conversely, glomeruli from CST^{Tg} mice presented downregulation of several genes of the ER stress and oxidative stress pathways as well as decreased expression of some pro-apoptotic genes (**Fig.9**).

Taken together, these results indicate that calpastatin overexpression could prevent glomerular injury by reducing AngII + HSD-induced ER and oxidative stress.

DISCUSSION

In the present study, we demonstrated that, in AngII + HSD-induced hypertension, podocyte autophagy is markedly downregulated. Furthermore, mice with podocyte-specific deletion of *Atg5* were more prone to AngII + HSD-induced glomerulosclerosis and podocyte loss, thus showing that autophagy in podocytes prevents development of hypertensive nephropathy, highlighting the critical role of autophagy in AngII + HSD-induced podocyte injury. Little is known about the extracellular stimuli that regulate cellular autophagy and these results shed light on the pathophysiological regulation of podocyte autophagy by AngII.

In most human glomerulopathies, podocyte foot process effacement is a hallmark of glomerular injury leading to proteinuria. Autophagy is likely to play an essential role in maintaining podocyte function because these terminally differentiated cells display high rates of autophagy even in the absence of stress. A previous study showed that AngII promotes autophagy through the generation of ROS in a conditionally immortalized murine podocyte cell line[60]. ROS production is indeed a general inducer of autophagy in many cell types and the reasons for such discrepancy with our findings are unclear. Unlike this latter study, we used murine primary cultured podocytes retaining

Podocin and Nephrin expression, and *in vivo* approaches and not murine cell line. We confirm previous reports that postmitotic podocytes exhibit an unusually high level of constitutive autophagy. Measurement of increased amount of LC3-II after AngII stimulation in the presence or absence of lysosomal inhibitors is necessary to determine if the autophagic flux is increased or blocked. Previous studies have neglected this phenomenon[60].

Here, we used a hypertensive model based on AngII perfusion and high salt diet. Podocyte exhibit AT1 receptor and are exposed to freely filtered peptides such as AngII[13, 16, 26, 61-65]. It is assumed that the observed renoprotective effects of RAAS inhibition could be – at least partially – due to a blockade of this podocyte-specific RAAS. Likewise, *in vivo* studies confirmed the effect of AngII on podocyte injury and podocyte-specific gene targeting of AT1 demonstrated that activation of AT1 receptors in the glomerulus in experimental lupus nephritis is sufficient to accelerate renal injury in the absence of hypertension[66, 67]. Calpain-mediated autophagy dysregulation in our model could be linked to a direct AngII-AT1 signaling on podocyte or to be a consequence of hypertension. We may provide an early answer to this question. Indeed, in the DOCA-salt model, we also found P62 accumulation in podocyte from hypertensive mice (**Fig.S3**). This suggests that autophagy blockade occurs in podocyte in this model, which is supposed to be independent of AngII[68]. Further studies evaluating podocyte injury pertaining to calpain activity and autophagic flux in mice deficient for AT1 in podocyte selectively would be required to delineate if such regulation of podocyte autophagy depends on direct or indirect effects of AngII.

Calpains 1 and 2 are ubiquitous pro-inflammatory proteases, whose activity is controlled by calpastatin, their specific inhibitor. Indeed, calpastatin inhibits selectively calpains and no other proteases to date. Calpain activation has been linked recently to renal injury in several pathological contexts[69,70]. The calcium channel transporter Transient receptor potential channel C6 (TRPC6) was found to activate calpain-1 in podocyte *via* a Ca2+/calcineurin activation. Kidneys of patients with FSGS had increased TRPC6 expression, increased calpain and calcineurin activity, and reduced

expression of the calpain target Talin-1, which is critical for podocyte cytoskeletal stability [71]. TRPC6 also directly binds to calpain-1 and calpain-2. This interaction is crucial for the regulation of Talin-1 cleavage and control motility of podocytes[72].

Transgenic mice over-expressing calpastatin are protected against vascular remodeling and AngII-dependent inflammation[73], against inflammation in models of glomerulonephritis[43], sepsis[74] or allograft rejection[75] and against aged-related inflammation[76]. Podocyte injury in these mice has not been explored. Letavernier et al. showed that overexpression of CST prevented AngII-dependent perivascular inflammation in kidneys[43]. Thus, renal protection in CST^{Tg} mice could be mediated, at least partially, by an anti-inflammatory mechanism. We evaluate macrophages and lymphocytes infiltration in our model and found no significant difference in renal inflammation between CST^{Tg} and control mice when analyzing global renal leukocyte infiltration (**Fig.S6**).

Calpain were involved recently in autophagy regulation (reviewed recently in Weber 2019[53]) with interesting endothelio-protective properties of calpain inhibition in diabetic context through restoration of autophagy[77]. Here, we reported that calpain inhibition through calpastatin overexpression prevented i) podocyte injury during hypertension and ii) restore autophagy in podocytes, thus highlighting a novel deleterious role of calpain activation during hypertension through the inhibition of autophagy.

Nearly all ATG proteins were shown to be cleaved by calpains *in vitro*[78]. Here we postulated that autophagy maintenance in hypertensive CST^{Tg} mice was mediated by calpain inhibition. To support our hypothesis, we showed that podocytes from CST^{Tg} have a decreased calpain activity when challenged with AngII *in vitro* (**Fig.3C**). We found increased ATG5 protein level in podocytes from CST^{Tg} mice, which suggest that calpastatin overexpression prevented calpain-mediated ATG5 cleavage in this context (**Fig.5A**). On the other hand, it was demonstrated that CST-mediated calpains inhibition could be independent of the inhibition of their protease activity[79], thus we could not exclude a regulation of autophagy by calpastatin independent to calpain enzymatic activity.

In summary, these findings revealed a previously unrecognized role for calpastatin in the regulation of podocyte autophagy and provide a lead for investigation of novel therapeutic strategies to enhance podocyte survival during hypertensive nephropathies.

DISCLOSURE

The authors declare no competing financial interests.

ACKNOWLEDGMENTS

This work was supported by the Institut National de la Santé Et de la Recherche Médicale (Inserm) and Université de Paris. I.B. was supported by a graduate fellowship from the Ministère de l'Education Nationale, de la Recherche et de la Technologie. O.L. was funded through an European Foundation for the Study of Diabetes (EFSD) award supported by EFSD/Novo Nordisk Programme for Diabetes Research in Europe and a grant from the Société Francophone du Diabète (SFD). B.R and C.H were funded by Starting Grant 107037 from European Research Council and the European Union (P-L.T). Y.S. was supported by a graduate fellowship from the Fondation de France.

We thank Elizabeth Huc, Nicolas Perez, Corina Suldac and the ERI U970 team for assistance in animal care and handling, Nicolas Sorhaindo for biochemical measurements (ICB-IFR2, laboratoire de Biochimie, Hôpital Bichat, Paris, France) and Alain Schmitt and Jean-Marc Masse for transmission electron microscopy (Institut Cochin, Paris, France). We thank Morgane Le Gall (Cochin proteomic facility 3P5) for help on *in silico* analysis. We acknowledge administrative support from Véronique Oberweis, Bruno Pillard and Cyrille Mahieux.

SUPPLEMENTARY MATERIALS

Figure S1: Primary podocyte culture expresses podocyte markers. Western blot analysis of the expression of the podocyte markers NPHS1 and NPHS2 in primary podocyte culture from WT and *CST*^{Tg} mice. Tubulin (TUBA) serves as a loading control. Representataive of n=4 mice per genotype**.**

Figure S2: High basal level of podocyte autophagy. (A-B) Representative immunofluorescence images of the expression of GFP (green) and NPHS1 (red) in glomeruli from *GFP-LC3* mice treated or not with CQ (80mg/kg) 4 hours before to sacrifice. Arrowheads show GFP+ autophagosomes. (C-D) Representative immunofluorescence images of the expression of GFP (green) and P62 (red) in glomeruli from GFP-LC3 mice treated or not with CQ (80mg/kg) 4 hours before to sacrifice. Arrowheads show GFP+ P62+ autophagosomes. (A-D) (') represent higher magnification. Nuclei were stained with Hoechst (blue). Scale bar: 50µm. N=4 mice per condition (E-H) Representative immunofluorescence images of the expression of GFP (green) and P62 (red) in primary podocyte from *GFP-LC3* mice treated (F, H) or not (E, G) with Bafilomycin A1 (100nM) for 4 hours. N=5 mice per condition.

Figure S3: P62 accumulates in podocytes in the DOCA-salt model of hypertension. (A-C) Representative immunofluorescence images of the expression of P62 (green) and PODXL (red) in glomeruli from WT mice after 2-to-6 weeks of DOCA-salt model. (') represent higher magnification. Nuclei were stained with Hoechst (blue). Scale bar: 50µm. (D) Quantification of P62 area per podocyte area (%). N=5-6 mice per condition. One-way ANOVA: Time p=0.0059, Sidak's multiple comparison test: D42 *vs.* D14 ** p=0.0055, D28 *vs.* D14 p=0.8590

Figure S4: Podocyte autophagy is dispensable for podocyte development. (A) Systolic blood pressure, (B) urine albumin-to-creatinine ratio and (C) blood urea nitrogen levels in *Atg5*$^{lox/lox}$ and *Nphs2.cre Atg5*$^{lox/lox}$ mice. N= 5-6 mice per genotype. Values are presented as individual plots and

means +/- sem. Mann-Whitney test: p=0.7273 (A), p=04286 (B), p=0.6623 (C). (D-E) Representative images of Masson's trichrome-stained sections of glomeruli from *Atg5*$^{lox/lox}$ and *Nphs2.cre Atg5*$^{lox/lox}$ mice. (F-G) Representative immunofluorescence images of the expression of PODXL (green) and WT1 (red) in *Atg5*$^{lox/lox}$ and *Nphs2.cre Atg5*$^{lox/lox}$ mice. Nuclei were stained with Hoechst (blue). (D-G) Scale bar: 50µm. N=6 mice per genotype (H-I) Representative photomicrographs of transmission electron microscopy sections of glomeruli from *Atg5*$^{lox/lox}$ and *Nphs2*.cre *Atg5*$^{lox/lox}$ mice. Scale bar: 1µm. N=3 mice per genotype.

Figure S5: Calpastatin overexpression does not influence renal function at baseline. (A) blood urea nitrogen and (B) plasma albumin levels in 12-weeks old *GFP-LC3* and *CST*^{Tg} *GFP-LC3* mice. N= 5 *GFP-LC3* and N=6 *CST*^{Tg} *GFP-LC3*. Values are presented as individua plots and means +/- sem. Mann-Whitney test: p=0.6623 (A) and p=0.9307 (B). (C-D) Representative images of Masson's trichrome-stained sections of glomeruli from *GFP-LC3* and *CST*^{Tg} *GFP-LC3* mice. (E-H) Representative immunofluorescence images of the expression of PODXL (E-F) and NPHS1 (G-H) in *GFP-LC3* and *CST*^{Tg} *GFP-LC3* mice. (C-H) Scale bar: 50µm. (I-J) Associated quantification of PODXL and NPHS1 area per glomerular section. N= 5 *GFP-LC3* and N=6 *CST*^{Tg} *GFP-LC3*. Values are presented as individual plots and means +/- sem. Mann-Whitney test: p= 0.1898 (A) and p= 0.8413 (B).

Figure S6: Calpastatin overexpression does not influence global renal inflammation. Representative immunohistochemistry of the expression of F4/80 (A-B) and CD3 (D-E) in *GFP-LC3* and *CST*^{Tg} *GFP-LC3* mice after 6 weeks of Angiotensin II +HSD. Scale bar: 200µm. (C, F) Associated quantification of F4/80 and CD3 area per kidney section. N=7 CST^{Tg} GFP-LC3 and N=8 GFP-LC3 mice. Values are presented as individual plots and means +/- sem. Mann-Whitney test: p=0.3969 (C) p=0.3357 (F).

Figure S7: Podocyte autophagy deficiency does not induce ER stress or oxidative stress in young adult at baseline. qPCR analysis of the mRNA expression of genes of the ER stress, oxidative stress

and apoptosis pathway by Qiagen qPCR array in glomeruli from WT and *Nphs2.cre Atg5*$^{lox/lox}$ mice (A) and WT and *CST*^{Tg} mice (B). N=4 mice per genotype. For *Nox3*, Ct >33.

Supplementary Table 1: *In silico* prevision of calpain cleavage sites. Calpain cleavage sites were predicted in podocyte-related and autophagy-related proteins with GPS-CCD (http://ccd.biocuckoo.org), CaMPDB (http://calpain.org) and DeepCalpain Predict (http://deepcalpain.cancerbio.info/help.php)

Supplementary File 1: Full file of *in silico* prevision of calpain cleavage sites. Calpain cleavage sites were predicted in podocyte-related and autophagy-related proteins with GPS-CCD (http://ccd.biocuckoo.org), CaMPDB (http://calpain.org) and DeepCalpain Predict (http://deepcalpain.cancerbio.info/help.php). Prediction cleavage sites are resumed for each protein for GPS-CCD and DeepCalpain Predict.

FIGURE LEGENDS

Figure 1: Angiotensin II +HSD-induced hypertension inhibits glomerular autophagy

(A-C) Immunofluorescence of PODXL (red) and P62 (green) in glomeruli from WT mice (A, A'), from WT mice after 6 weeks of Angiotensin II +HSD (B, B') and from *Nphs2*.cre *Atg5*$^{lox/lox}$ mice (C, C') showing accumulation of P62 in podocyte during hypertension and in podocyte-specific ATG5 deficient mice. P62+ dots are shown with arrowheads in the WT in (A'). Nuclei were counterstained with Hoechst (blue). (') represents higher magnification. Scale bar: 50 µm. (D) Associated quantification of the P62+ area expressed as the percentage of glomerular area. N= 4 WT and N=5 WT with angiotensin II +HSD and *Nphs2*.cre *Atg5*$^{lox/lox}$ mice. Values are presented as individual plots and mean +/- sem. * p=0.0159, Mann-Whitney test.

Figure 2: Deletion of *Atg5* specifically in podocytes results in a significant increase in albuminuria, kidney injury and podocyte loss after 6 weeks of AngII infusion + HSD

(A) Systolic blood pressure in *Atg5*$^{lox/lox}$ and *Nphs2*.cre *Atg5*$^{lox/lox}$ mice during 36 days of Angiotensin II +HSD. N=9 mice per genotype. Values are presented as mean +/- sem. Two-way ANOVA: ns. From (B) to (M), N= 10 mice per genotype. In (B, G, H, K) values are presented as individual plots and mean +/- sem. (B) Angiotensin II +HSD resulted in a dramatic increase of albuminuria in *Nphs2*.cre *Atg5*$^{lox/lox}$ mice compared with *Atg5*$^{lox/lox}$ control mice. Two-way ANOVA: Genotype p=0.013, Time p=0.0018. (C-F) Representative images of Masson's trichrome–stained sections of glomeruli from *Atg5*$^{lox/lox}$ control and *Nphs2*.cre *Atg5*$^{lox/lox}$ mice after 6 weeks of Angiotensin II +HSD. Scale bar : 50 µm in (C-D) and 100 µm in (E-F). (G-H) Comparison of the proportion of sclerotic glomeruli (G) and of the number of tubular casts per microscope field (H). Mann-Whitney test: ** p=0.0026 in (H) *** p=0.0003 in (G). (I-J) Representative immunofluorescence images of the expression of WT1 (red) and PODXL (green) in glomeruli from *Atg5*$^{lox/lox}$ control and *Nphs2*.cre *Atg5*$^{lox/lox}$ mice after angiotensin II +HSD for 6 weeks. Nuclei were stained with Hoechst (blue). Scale bar: 50 µm. (K) Quantification of the number of WT1-positive cells per glomerular sections. Mann-Whitney test: ** p=0.0029 (L-M) Representative immunofluorescence images of the expression of CD44 (green) in glomeruli from *Atg5*$^{lox/lox}$ control and *Nphs2*.cre *Atg5*$^{lox/lox}$ mice after angiotensin II +HSD for 6 weeks. Nuclei were stained with Hoechst (blue). Scale bar: 50 µm. (N-O) Representative photomicrographs of transmission electron microscopy sections of glomeruli from *Atg5*$^{lox/lox}$ control and *Nphs2*.cre *Atg5*$^{lox/lox}$ mice after angiotensin II +HSD for 6 weeks; showing podocyte foot process effacement (arrowhead) in *Nphs2*.cre *Atg5*$^{lox/lox}$ hypertensive mice. Scale bar: 1 µm. N=3 mice per genotype.

Figure 3: Calpain expression and activity in podocytes

(A) Western blot analysis of the expression of Calpain 1, Calpain 2 and Calpain 4 in primary podocytes. Tubulin (TUBA) expression serves as normalization. (B) Calpain activity was measured on primary podocyte treated or not with AngII (100nM) for 24 hours with or without calpeptin (10µM). N=5

independent experiments. Values are presented as individual plots and mean +/- sem. One-way ANOVA: Treatment p=0.0035, Sidak's multiple comparison test: * p=0.0128 AngII *vs.* Baseline ## p=0.0056 AngII + calpeptin *vs.* AngII (C) Calpain activity was measured on primary podocyte from WT or CST^{Tg} mice treated or not with AngII (100nM) for 24 hours. N=7 independent experiments. Values are presented as individual plots and mean +/- sem. Two-way ANOVA paired for treatment: Genotype p=0.0483, Sidak's multiple comparison test: *** p=0.0009 for WT AngII *vs.* Baseline *p=0.0420 for CST^{Tg} AngII *vs.* Baseline. # p=0.0424 WT vs. CST^{Tg} AngII.

Figure 4: Evaluation of the autophagic flux in podocyte of CST^{Tg} mice

(A-B) Representative immunofluorescence images of the expression of GFP (green) and P62 (red) in glomeruli from 12 weeks-old *GFP-LC3* and *CST^{Tg} GFP-LC3* mice. Arrowheads show GFP+ P62+ autophagosomes (C-D) Representative immunofluorescence images of the expression of P62 (green) and PODXL (red) in glomeruli from 12 weeks-old *GFP-LC3* and *CST^{Tg} GFP-LC3* mice. (') represents higher magnification. Nuclei were stained with Hoechst (blue). Scale bar: 50 µm. (E) Quantification of the number of LC3+ P62+ dots per podocyte. Mann-Whitney test: ** p=0.0065 (F) Quantification of P62+ area per glomerular section. Mann-Whitney test: * p=0.0420. In (E, F) N=5 *GFP-LC3* and N=8 *CST^{Tg} GFP-LC3* mice. Values are presented as individual plots and mean +/- sem.

Figure 5: Blocking autophagosomal degradation confirmed increased podocyte autophagic flux in CST^{Tg} mice

(A) Western blot analysis of the expression of LC3, SQSTM1/P62 and ATG5 in primary podocyte from WT or CST^{Tg} mice. Tubulin (TUBA) expression serves as normalization. Podocyte were treated or not with bafilomycin A1 (100nM) for 4 hours before culture arrest (B) Quantification of the LC3 II/ Tubulin and P62/tubulin ratios. N= 10 WT and 8 CST^{Tg} mice. Values are presented as individual plots and mean +/- sem. Two-way ANOVA paired for treatment: for LC3 II/Tubulin Genotype p=0.0008 Treatment p<0.0001 and for P62/Tubulin Genotype p=0.0884 Treatment p<0.0001. Sidak's multiple

comparison test: for LC3 II/Tubulin *** p<0.0001 WT -BafA1 *vs.* WT +BafA1, *** p<0.0001 CST^{Tg} -BafA1 vs. CST^{Tg} +BafA1, ## p=0.0028 WT +BafA1 *vs.* CST^{Tg} +BafA1 and for P62/Tubulin *** p<0.0001 WT -BafA1 *vs.* WT +BafA1, *** p<0.0001 CST^{Tg} -BafA1 vs. CST^{Tg} +BafA1. (C-D) Representative immunofluorescence images of the expression of GFP (green) and P62 (red) in glomeruli from 12 weeks-old *GFP-LC3* and *CST^{Tg} GFP-LC3* mice. (') represents higher magnification. Nuclei were stained with Hoechst (blue). Scale bar: 50 µm. Mice were treated with CQ (80mg/kg) 4 hours before sacrifice. Arrowheads show GFP+ P62+ autophagosomes (E) Quantification of the number of LC3+ P62+ dots per podocyte. N=5 mice per genotype. Values are presented as individual plots and mean +/- sem. Unpaired t-test with equal SD: * p=0.0302

Figure 6: **Calpastatin overexpression prevents AngII + HSD-mediated podocyte injury**

(A-B) Representative images of Masson's trichrome–stained sections of glomeruli from WT and *CST^{Tg}* mice after 6 weeks of AngII +HSD. Scale bar: 50 µm. (C-G) Representative immunofluorescence images of the expression of PODXL (C-D) and NPHS1 (F-G) in WT and *CST^{Tg}* mice after 6 weeks of AngII +HSD and (E, H) associated quantifications. Scale bar: 50 µm. (I-J) Representative immunofluorescence images of the expression of WT1 (green) and PODXL (red) in glomeruli from WT and *CST^{Tg}* mice after 6 weeks of AngII +HSD and (K) associated quantification of the number of WT1+ cells per glomerular section. Nuclei were stained with Hoechst (blue). Scale bar: 50 µm. (E, H, K) Values are presented as individual plots and mean +/- sem. N= 9 WT and N=7 CST^{Tg} mice. Unpaired t-test with equal SD: ** p=0.0095 (E), * p=0.0249 (H), p=0.7891 (K).

Figure 7: **Calpastatin overexpression prevents AngII + HSD-mediated podocyte injury in GFP-LC3 mice**

(A) AngII +HSD resulted in a dramatic increase of albuminuria in *GFP-LC3* mice compared with *CST^{Tg} GFP-LC3* mice. N=8-13 mice per genotype. Values are presented as individual plots and mean +/- sem. Two-way ANOVA Genotype *p=0.0429 Time p=0.0165. Sidak's multiple comparison test: * p=0.0453

GFP-LC3 vs. *CST*^{Tg} *GFP-LC3* at day 28. (B-C) Representative immunofluorescence images of the expression of WT1 (green) and nephrin (red) in glomeruli from 18 weeks-old *GFP-LC3* and *CST*^{Tg} *GFP-LC3* mice after 6 weeks of AngII infusion + HSD. Nuclei were stained with Hoechst (blue). Scale bar: 50 µm. Quantification of nephrin (NPHS1) area per glomerular section (D) and of the number of WT1+ cells per glomerular section (E) in 18 weeks-old *GFP-LC3* and *CST*^{Tg} *GFP-LC3* mice after 6 weeks of AngII infusion + HSD. N=19 *GFP-LC3* and N=25 *CST*^{Tg} *GFP-LC3* mice. Values are presented as individual plots and mean +/- sem. Unpaired t-test with equal SD: ** p=0.0010 (D) p=0.1158 (E). (F-G) Transmission electron microscopy images of glomeruli from *GFP-LC3* and *CST*^{Tg} *GFP-LC3* mice after 6 weeks of AngII +HSD. Arrowheads show foot process effacement. Scale bar: 1 µm (H) Quantification of the number of foot process per µm of GBM. N=3 mice per genotype. Values are presented as individual plots and mean +/- sem. Each plot represents the mean number of podocyte per µm of GBM on one continuous length of GBM. Unpaired t-test with equal SD: p=0.7512.

Figure 8: Calpastatin overexpression prevents AngII + HSD-induced autophagy downregulation in podocytes

(A-B) Representative immunofluorescence images of the expression of P62 (green) and PODXL (red) in glomeruli from *GFP-LC3* and *CST*^{Tg} *GFP-LC3* mice after 6 weeks of AngII +HSD. (‘) represents higher magnification. Nuclei were stained with Hoechst (blue). Scale bar: 50 µm. (C-D) Quantification of P62+ area per glomerular section. N=9 WT and N=7 *CST*^{Tg} mice in (C) and N=16 *GFP-LC3* and N=16 *CST*^{Tg} *GFP-LC3* in (D). Values are presented as individual plots and mean +/- sem. Mann-Whitney test: ** p=0.0033 (C) and ** p=0.0011 (D). (E-F) Representative immunofluorescence images of the expression of GFP (green) and P62 (red) in glomeruli from *GFP-LC3* and *CST*^{Tg} *GFP-LC3* mice after 6 weeks of AngII +HSD. (‘) represents higher magnification. Arrowheads show GFP+ P62+ autophagosomes. (G) Quantification of the number of LC3+ P62+ dots per podocyte. N=11 *GFP-LC3* and N=16 *CST*^{Tg} *GFP-LC3*. Values are presented as individual plots and mean +/- sem. Unpaired t-test with equal SD: p= 0.1014

Figure 9: Glomerular ER stress and oxidative stress

(A) qPCR analysis of the mRNA expression of genes of the ER stress, oxidative stress and apoptosis pathway by Qiagen qPCR array in glomeruli from WT, *Nphs2.cre Atg5*$^{lox/lox}$ and *CST*^{Tg} mice after 6 weeks of AngII +HSD. Data are represented as a heatmap of the Log2(fold change) in gene expression. N=5 mice per genotype (B) Representation of the genes significantly upregulated or downregulated in *Nphs2.cre Atg5*$^{lox/lox}$ vs. WT mice. (C) Representation of the genes significantly upregulated or downregulated in *CST*^{Tg} vs. WT mice. (B,C) Unpaired t-test with equal SD $p < 0.05$.

REFERENCES

1. Coresh J, Selvin E, Stevens LA*, et al.* Prevalence of chronic kidney disease in the United States. *Jama* 2007; **298:** 2038-2047.

2. Collins AJ, Vassalotti JA, Wang C*, et al.* Who should be targeted for CKD screening? Impact of diabetes, hypertension, and cardiovascular disease. *Am J Kidney Dis* 2009; **53:** S71-77.

3. Chang TI, Li S, Chen SC*, et al.* Risk factors for ESRD in individuals with preserved estimated GFR with and without albuminuria: results from the Kidney Early Evaluation Program (KEEP). *American journal of kidney diseases : the official journal of the National Kidney Foundation* 2013; **61:** S4-11.

4. Hsu CY, McCulloch CE, Darbinian J*, et al.* Elevated blood pressure and risk of end-stage renal disease in subjects without baseline kidney disease. *Arch Intern Med* 2005; **165:** 923-928.

5. Nagase M, Shibata S, Yoshida S*, et al.* Podocyte injury underlies the glomerulopathy of Dahl salt-hypertensive rats and is reversed by aldosterone blocker. *Hypertension* 2006; **47:** 1084-1093.

6. Garovic VD, Wagner SJ, Turner ST*, et al.* Urinary podocyte excretion as a marker for preeclampsia. *Am J Obstet Gynecol* 2007; **196:** 320 e321-327.

7. Craici IM, Wagner SJ, Bailey KR*, et al.* Podocyturia predates proteinuria and clinical features of preeclampsia: longitudinal prospective study. *Hypertension* 2013; **61:** 1289-1296.

8. Wang G, Lai FM, Kwan BC*, et al.* Podocyte loss in human hypertensive nephrosclerosis. *Am J Hypertens* 2009; **22:** 300-306.

9. Wang G, Kwan BC, Lai FM*, et al.* Intrarenal expression of miRNAs in patients with hypertensive nephrosclerosis. *American journal of hypertension* 2010; **23:** 78-84.

10. Ruggenenti P, Perna A, Gherardi G*, et al.* Chronic proteinuric nephropathies: outcomes and response to treatment in a prospective cohort of 352 patients with different patterns of renal injury. *American journal of kidney diseases : the official journal of the National Kidney Foundation* 2000; **35:** 1155-1165.

11. Fukuda A, Wickman LT, Venkatareddy MP*, et al.* Angiotensin II-dependent persistent podocyte loss from destabilized glomeruli causes progression of end stage kidney disease. *Kidney international* 2011.

12. Tuncdemir M, Ozturk M. The effects of angiotensin-II receptor blockers on podocyte damage and glomerular apoptosis in a rat model of experimental streptozotocin-induced diabetic nephropathy. *Acta Histochem* 2011; **113:** 826-832.

13. Nijenhuis T, Sloan AJ, Hoenderop JG*, et al.* Angiotensin II contributes to podocyte injury by increasing TRPC6 expression via an NFAT-mediated positive feedback signaling pathway. *Am J Pathol* 2011; **179:** 1719-1732.

14. EUCLID. Randomised placebo-controlled trial of lisinopril in normotensive patients with insulin-dependent diabetes and normoalbuminuria or microalbuminuria. The EUCLID Study Group. *Lancet* 1997; **349:** 1787-1792.

15. de Zeeuw D, Remuzzi G, Parving HH*, et al.* Proteinuria, a target for renoprotection in patients with type 2 diabetic nephropathy: lessons from RENAAL. *Kidney Int* 2004; **65:** 2309-2320.

16. Benigni A, Gagliardini E, Remuzzi G. Changes in glomerular perm-selectivity induced by angiotensin II imply podocyte dysfunction and slit diaphragm protein rearrangement. *Semin Nephrol* 2004; **24:** 131-140.

17. Wang L, Flannery PJ, Spurney RF. Characterization of angiotensin II-receptor subtypes in podocytes. *The Journal of laboratory and clinical medicine* 2003; **142:** 313-321.

18. Langham RG, Kelly DJ, Cox AJ*, et al.* Proteinuria and the expression of the podocyte slit diaphragm protein, nephrin, in diabetic nephropathy: effects of angiotensin converting enzyme inhibition. *Diabetologia* 2002; **45:** 1572-1576.

19. Nakamura T, Ushiyama C, Suzuki S*, et al.* Effects of angiotensin-converting enzyme inhibitor, angiotensin II receptor antagonist and calcium antagonist on urinary podocytes in patients with IgA nephropathy. *American journal of nephrology* 2000; **20:** 373-379.

20. Henger A, Huber T, Fischer KG*, et al.* Angiotensin II increases the cytosolic calcium activity in rat podocytes in culture. *Kidney international* 1997; **52:** 687-693.

21. Praga M, Hernandez E, Montoyo C*, et al.* Long-term beneficial effects of angiotensin-converting enzyme inhibition in patients with nephrotic proteinuria. *American journal of kidney diseases : the official journal of the National Kidney Foundation* 1992; **20:** 240-248.

22. Nitschke R, Henger A, Ricken S*, et al.* Angiotensin II increases the intracellular calcium activity in podocytes of the intact glomerulus. *Kidney Int* 2000; **57:** 41-49.

23. Gloy J, Henger A, Fischer KG*, et al.* Angiotensin II modulates cellular functions of podocytes. *Kidney Int Suppl* 1998; **67:** S168-170.

24. Miceli I, Burt D, Tarabra E*, et al.* Stretch reduces nephrin expression via an angiotensin II-AT(1)-dependent mechanism in human podocytes: effect of rosiglitazone. *American journal of physiology Renal physiology* 2010; **298:** F381-390.

25. Endlich N, Endlich K. Stretch, tension and adhesion - adaptive mechanisms of the actin cytoskeleton in podocytes. *Eur J Cell Biol* 2006; **85:** 229-234.

26. Durvasula RV, Petermann AT, Hiromura K*, et al.* Activation of a local tissue angiotensin system in podocytes by mechanical strain. *Kidney Int* 2004; **65:** 30-39.

27. Riser BL, Cortes P, Heilig C*, et al.* Cyclic stretching force selectively up-regulates transforming growth factor-beta isoforms in cultured rat mesangial cells. *The American journal of pathology* 1996; **148:** 1915-1923.

28. Kretzler M, Koeppen-Hagemann I, Kriz W. Podocyte damage is a critical step in the development of glomerulosclerosis in the uninephrectomised-desoxycorticosterone hypertensive rat. *Virchows Archiv : an international journal of pathology* 1994; **425:** 181-193.

29. Jung HS, Chung KW, Won Kim J*, et al.* Loss of autophagy diminishes pancreatic beta cell mass and function with resultant hyperglycemia. *Cell Metab* 2008; **8:** 318-324.

30. Ebato C, Uchida T, Arakawa M*, et al.* Autophagy is important in islet homeostasis and compensatory increase of beta cell mass in response to high-fat diet. *Cell Metab* 2008; **8:** 325-332.

31. Lenoir O, Jasiek M, Henique C*, et al.* Endothelial cell and podocyte autophagy synergistically protect from diabetes-induced glomerulosclerosis. *Autophagy* 2015; **11:** 1130-1145.

32. Hartleben B, Godel M, Meyer-Schwesinger C*, et al.* Autophagy influences glomerular disease susceptibility and maintains podocyte homeostasis in aging mice. *J Clin Invest* 2010; **120:** 1084-1096.

33. Sato S, Kitamura H, Adachi A*, et al.* Two types of autophagy in the podocytes in renal biopsy specimens: ultrastructural study. *J Submicrosc Cytol Pathol* 2006; **38:** 167-174.

34. Asanuma K, Tanida I, Shirato I*, et al.* MAP-LC3, a promising autophagosomal marker, is processed during the differentiation and recovery of podocytes from PAN nephrosis. *FASEB J* 2003; **17:** 1165-1167.

35. Mizushima N, Levine B, Cuervo AM*, et al.* Autophagy fights disease through cellular self-digestion. *Nature* 2008; **451:** 1069-1075.

36. Yang L, Li P, Fu S*, et al.* Defective hepatic autophagy in obesity promotes ER stress and causes insulin resistance. *Cell Metab* 2010; **11:** 467-478.

37. Xie Z, Klionsky DJ. Autophagosome formation: core machinery and adaptations. *Nature cell biology* 2007; **9:** 1102-1109.

38. Kume S, Thomas MC, Koya D. Nutrient sensing, autophagy, and diabetic nephropathy. *Diabetes* 2012; **61:** 23-29.

39. Kume S, Uzu T, Maegawa H*, et al.* Autophagy: a novel therapeutic target for kidney diseases. *Clin Exp Nephrol* 2012; **16:** 827-832.

40. Huber TB, Edelstein CL, Hartleben B*, et al.* Emerging role of autophagy in kidney function, diseases and aging. *Autophagy* 2012; **8:** 1009-1031.

41. Weide T, Huber TB. Implications of autophagy for glomerular aging and disease. *Cell Tissue Res* 2011; **343:** 467-473.

42. Bork T, Liang W, Yamahara K*, et al.* Podocytes maintain high basal levels of autophagy independent of mtor signaling. *Autophagy* 2019**:** 1-17.

43. Peltier J, Bellocq A, Perez J*, et al.* Calpain activation and secretion promote glomerular injury in experimental glomerulonephritis: evidence from calpastatin-transgenic mice. *J Am Soc Nephrol* 2006; **17:** 3415-3423.

44. Moeller MJ, Sanden SK, Soofi A*, et al.* Podocyte-specific expression of cre recombinase in transgenic mice. *Genesis* 2003; **35:** 39-42.

45. Hara T, Nakamura K, Matsui M*, et al.* Suppression of basal autophagy in neural cells causes neurodegenerative disease in mice. *Nature* 2006; **441:** 885-889.

46. Lazareth H, Henique C, Lenoir O*, et al.* The tetraspanin CD9 controls migration and proliferation of parietal epithelial cells and glomerular disease progression. *Nat Commun* 2019; **10:** 3303.

47. Bollee G, Flamant M, Schordan S*, et al.* Epidermal growth factor receptor promotes glomerular injury and renal failure in rapidly progressive crescentic glomerulonephritis. *Nat Med* 2011; **17:** 1242-1250.

48. Lenoir O, Milon M, Virsolvy A*, et al.* Direct action of endothelin-1 on podocytes promotes diabetic glomerulosclerosis. *J Am Soc Nephrol* 2014; **25:** 1050-1062.

49. Henique C, Bollee G, Lenoir O*, et al.* Nuclear Factor Erythroid 2-Related Factor 2 Drives Podocyte-Specific Expression of Peroxisome Proliferator-Activated Receptor gamma Essential for Resistance to Crescentic GN. *J Am Soc Nephrol* 2016; **27:** 172-188.

50. Perez J, Dansou B, Herve R*, et al.* Calpains Released by T Lymphocytes Cleave TLR2 To Control IL-17 Expression. *Journal of immunology* 2016; **196:** 168-181.

51. Raimbourg Q, Perez J, Vandermeersch S*, et al.* The calpain/calpastatin system has opposing roles in growth and metastatic dissemination of melanoma. *PloS one* 2013; **8:** e60469.

52. Letavernier B, Zafrani L, Nassar D*, et al.* Calpains contribute to vascular repair in rapidly progressive form of glomerulonephritis: potential role of their externalization. *Arterioscler Thromb Vasc Biol* 2012; **32:** 335-342.

53. Weber JJ, Pereira Sena P, Singer E*, et al.* Killing Two Angry Birds with One Stone: Autophagy Activation by Inhibiting Calpains in Neurodegenerative Diseases and Beyond. *BioMed research international* 2019; **2019:** 4741252.

54. Liu Z, Cao J, Gao X*, et al.* GPS-CCD: a novel computational program for the prediction of calpain cleavage sites. *PLoS One* 2011; **6:** e19001.

55. duVerle D, Takigawa I, Ono Y*, et al.* CaMPDB: a resource for calpain and modulatory proteolysis. *Genome Inform* 2010; **22:** 202-213.

56. Liu ZX, Yu K, Dong J*, et al.* Precise Prediction of Calpain Cleavage Sites and Their Aberrance Caused by Mutations in Cancer. *Front Genet* 2019; **10:** 715.

57. Yousefi S, Perozzo R, Schmid I*, et al.* Calpain-mediated cleavage of Atg5 switches autophagy to apoptosis. *Nat Cell Biol* 2006; **8:** 1124-1132.

58. Xia HG, Zhang L, Chen G*, et al.* Control of basal autophagy by calpain1 mediated cleavage of ATG5. *Autophagy* 2010; **6:** 61-66.

59. Russo R, Berliocchi L, Adornetto A*, et al.* Calpain-mediated cleavage of Beclin-1 and autophagy deregulation following retinal ischemic injury in vivo. *Cell Death Dis* 2011; **2:** e144.

60. Yadav A, Vallabu S, Arora S*, et al.* ANG II promotes autophagy in podocytes. *American journal of physiology Cell physiology* 2010; **299:** C488-496.

61. Flannery PJ, Spurney RF. Transactivation of the epidermal growth factor receptor by angiotensin II in glomerular podocytes. *Nephron Exp Nephrol* 2006; **103:** e109-118.

62. Harrison-Bernard LM, Navar LG, Ho MM*, et al.* Immunohistochemical localization of ANG II AT1 receptor in adult rat kidney using a monoclonal antibody. *The American journal of physiology* 1997; **273:** F170-177.

63. Liebau MC, Lang D, Bohm J*, et al.* Functional expression of the renin-angiotensin system in human podocytes. *American journal of physiology Renal physiology* 2006; **290:** F710-719.

64. Pavenstadt H. Franz Volhard Award 2000: angiotensin II signalling in the podocyte. *Kidney Blood Press Res* 2000; **23:** 156-158.

65. Wennmann DO, Hsu HH, Pavenstadt H. The renin-angiotensin-aldosterone system in podocytes. *Semin Nephrol* 2012; **32:** 377-384.

66. Jia J, Ding G, Zhu J*, et al.* Angiotensin II infusion induces nephrin expression changes and podocyte apoptosis. *American journal of nephrology* 2008; **28:** 500-507.

67. Crowley SD, Vasievich MP, Ruiz P*, et al.* Glomerular type 1 angiotensin receptors augment kidney injury and inflammation in murine autoimmune nephritis. *J Clin Invest* 2009; **119:** 943-953.

68. Song K, Stuart D, Abraham N*, et al.* Collecting Duct Renin Does Not Mediate DOCA-Salt Hypertension or Renal Injury. *PLoS One* 2016; **11:** e0159872.

69. Liu Z, Ji J, Zheng D*, et al.* Protective role of endothelial calpain knockout in lipopolysaccharide-induced acute kidney injury via attenuation of the p38-iNOS pathway and NO/ROS production. *Exp Mol Med* 2020; **52:** 702-712.

70. Seremwe M, Schnellmann RG, Bollag WB. Calpain-10 Activity Underlies Angiotensin II-Induced Aldosterone Production in an Adrenal Glomerulosa Cell Model. *Endocrinology* 2015; **156:** 2138-2149.

71. Verheijden KAT, Sonneveld R, Bakker-van Bebber M*, et al.* The Calcium-Dependent Protease Calpain-1 Links TRPC6 Activity to Podocyte Injury. *Journal of the American Society of Nephrology : JASN* 2018; **29:** 2099-2109.

72. Farmer LK, Rollason R, Whitcomb DJ*, et al.* TRPC6 Binds to and Activates Calpain, Independent of Its Channel Activity, and Regulates Podocyte Cytoskeleton, Cell Adhesion, and Motility. *J Am Soc Nephrol* 2019; **30:** 1910-1924.

73. Letavernier E, Perez J, Bellocq A*, et al.* Targeting the calpain/calpastatin system as a new strategy to prevent cardiovascular remodeling in angiotensin II-induced hypertension. *Circulation research* 2008; **102:** 720-728.

74. Zafrani L, Gerotziafas G, Byrnes C*, et al.* Calpastatin controls polymicrobial sepsis by limiting procoagulant microparticle release. *Am J Respir Crit Care Med* 2012; **185:** 744-755.

75. Letavernier E, Dansou B, Lochner M*, et al.* Critical role of the calpain/calpastatin balance in acute allograft rejection. *Eur J Immunol* 2011; **41:** 473-484.

76. Hanouna G, Mesnard L, Vandermeersch S*, et al.* Specific calpain inhibition protects kidney against inflammaging. *Scientific reports* 2017; **7:** 8016.

77. Ong SB, Lee WH, Shao NY*, et al.* Calpain Inhibition Restores Autophagy and Prevents Mitochondrial Fragmentation in a Human iPSC Model of Diabetic Endotheliopathy. *Stem Cell Reports* 2019; **12:** 597-610.

78. Norman JM, Cohen GM, Bampton ET. The in vitro cleavage of the hAtg proteins by cell death proteases. *Autophagy* 2010; **6:** 1042-1056.

79. De Tullio R, Averna M, Pedrazzi M*, et al.* Differential regulation of the calpain-calpastatin complex by the L-domain of calpastatin. *Biochim Biophys Acta* 2014; **1843:** 2583-2591.

Position	Refseq	Symbol	Description	RT2 Catalog
1	NM_013842	XBP1	X-box binding protein 1	PPM05627A
2	NM_009716	ATF4	Activating transcription factor 4	PPM04670A
3	NM_001081304	ATF6	Activating transcription factor 6	PPM33057A
4	NM_011631	HSP90B1	Heat shock protein 90, beta (Grp94), member 1	PPM05658A
5	NM_022310	HSP5A	Heat shock protein 5	PPM03586A
6	NM_007837	DDIT3	DNA-damage inducible transcript 3	PPM03736A
7	NM_138677	EDEM1	ER degradation enhancer, mannosidase alpha-like 1	PPM26189A
8	NM_008929	DNAJC3	DnaJ (Hsp40) homolog, subfamily C, member 3	PPM25697A
9	NM_007591	CALR	Calreticulin	PPM05020A
10	NM_022032	PERP	PERP, TP53 apoptosis effector	PPM04985A
11	NM_007522	BAD	BCL2-associated agonist of cell death	PPM02916A
12	NM_007527	BAX	Bcl2-associated X protein	PPM02917A
13	NM_009741	BCL2	B-cell leukemia/lymphoma 2	PPM02918A
14	NM_009761	BNIP3L	BCL2/adenovirus E1B interacting protein 3-like	PPM27647A
15	NM_009810	CASP3	Caspase 3	PPM02922A
16	NM_009812	CASP8	Caspase 8	PPM02923A
17	NM_011434	SOD1	Superoxide dismutase 1, soluble	PPM03582A
18	NM_198958	NOX3	NADPH oxidase 3	PPM40647A
19	NM_011198	PTGS2	Prostaglandin-endoperoxide synthase 2	PPM03647A
20	NM_011218	PTPRS	Protein tyrosine phosphatase, receptor type, S	PPM35547A
21	NM_023281	SDHA	Succinate dehydrogenase complex, subunit A, flavoprotein	PPM31938A
22	NM_008706	NQO1	NAD(P)H dehydrogenase, quinone 1	PPM03466A
23	NM_010442	HMOX1	Heme oxygenase (decycling) 1	PPM04356A
24	NM_008160	GPX1	Glutathione peroxidase 1	PPM04345A
25	NM_011034	PRDX1	Peroxiredoxin 1	PPM04383A
26	NM_010357	GSTA4	Glutathione S-transferase, alpha 4	PPM03928A
27	NM_009735	B2M	Beta-2 microglobulin	PPM03562A
28	NM_008084	GAPDH	Glyceraldehyde-3-phosphate dehydrogenase	PPM02946A
29	NM_007393	ACTB	Actin, beta	PPM02945A
30		MGDC	gDNA contamination control	PPM65836A
31		PPC	PCR array reproducibility control	PPX63339A
32	SA_00104	RTC	Reverse Transcription Control	PPX63340A

Table 1: Custom RT^2 qPCR Array

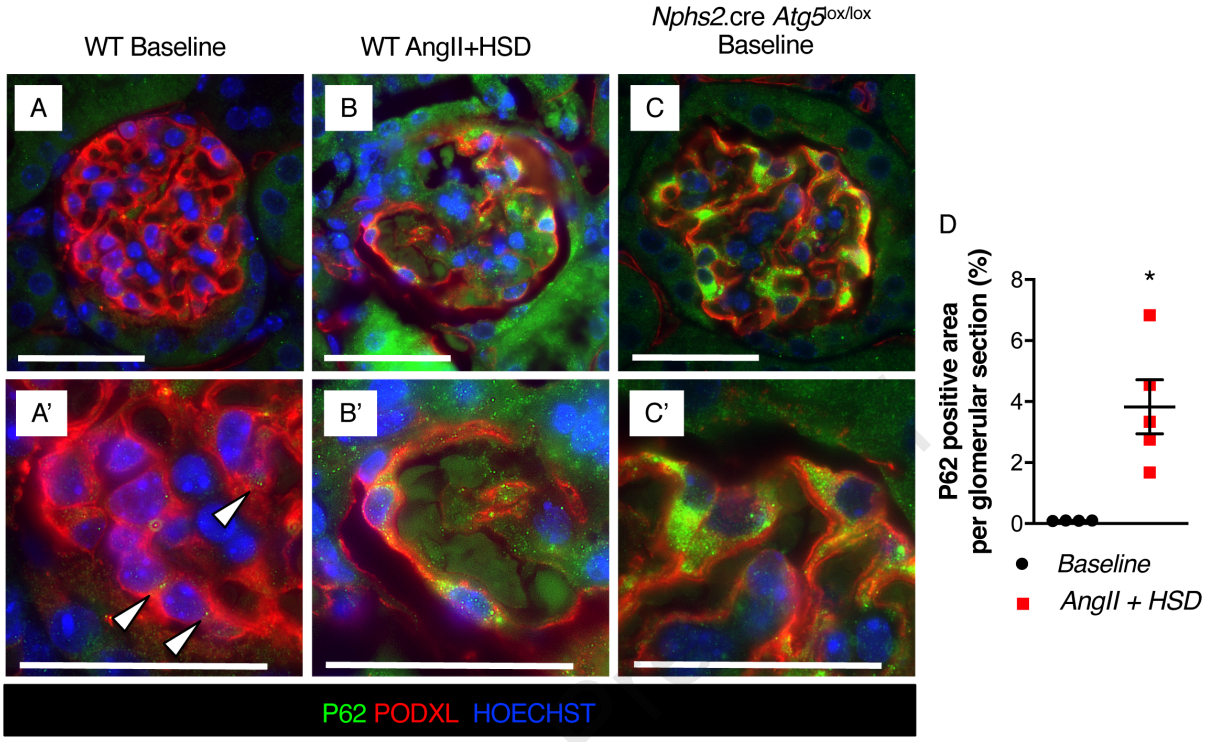

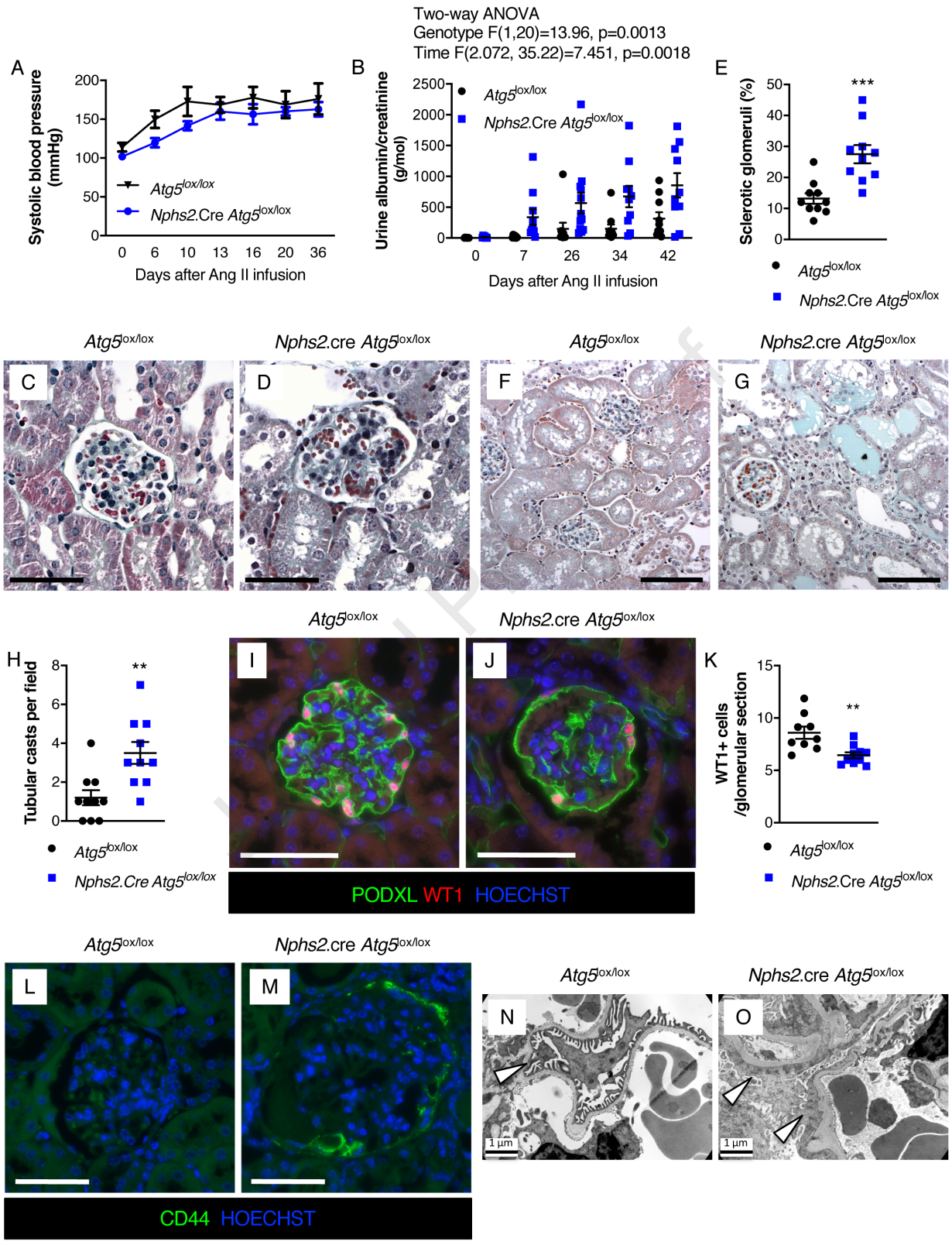
A
Systolic blood pressure (mmHg)
200
150
100
50
0
0 6 10 13 16 20 36
Days after Ang II infusion
Atg5lox/lox
Nphs2.Cre Atg5lox/lox
B
Two-way ANOVA
Genotype F(1,20)=13.96, p=0.0013
Time F(2.072, 35.22)=7.451, p=0.0018
Urine albumin/creatinine (g/mol)
2500
2000
1500
1000
500
0
0 7 26 34 42
Days after Ang II infusion
Atg5lox/lox
Nphs2.Cre Atg5lox/lox
E
Sclerotic glomeruli (%)
50
40
30
20
10
0
***
Atg5lox/lox
Nphs2.Cre Atg5lox/lox
Atg5lox/lox
Nphs2.cre Atg5lox/lox
C
D
Atg5lox/lox
Nphs2.cre Atg5lox/lox
F
G
H
Tubular casts per field
8
6
4
2
0
**
Atg5lox/lox
Nphs2.Cre Atg5lox/lox
Atg5lox/lox
Nphs2.cre Atg5lox/lox
I
J
PODXL WT1 HOECHST
K
WT1+ cells /glomerular section
15
10
5
0
**
Atg5lox/lox
Nphs2.Cre Atg5lox/lox
Atg5lox/lox
Nphs2.cre Atg5lox/lox
L
M
CD44 HOECHST
Atg5lox/lox
Nphs2.cre Atg5lox/lox
N
O
1 µm
1 µm

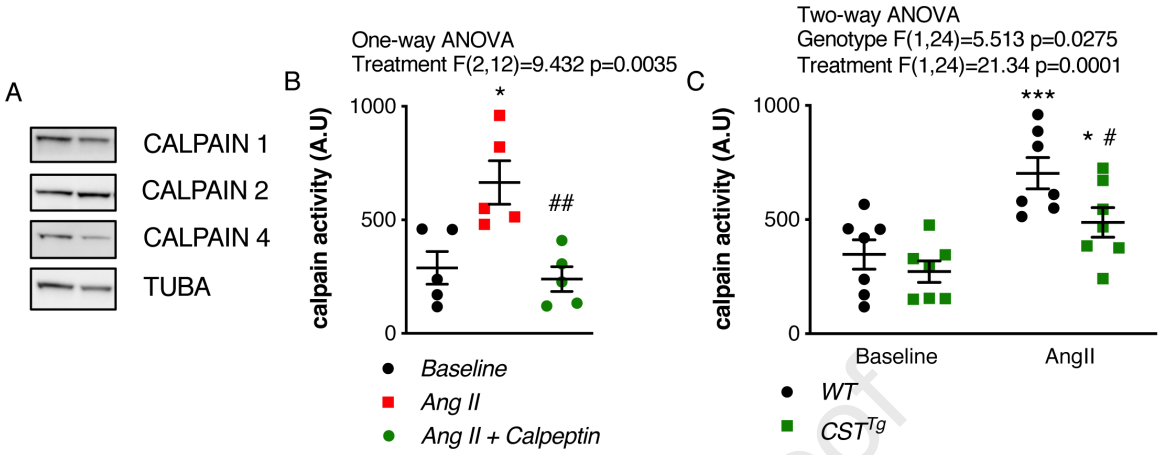

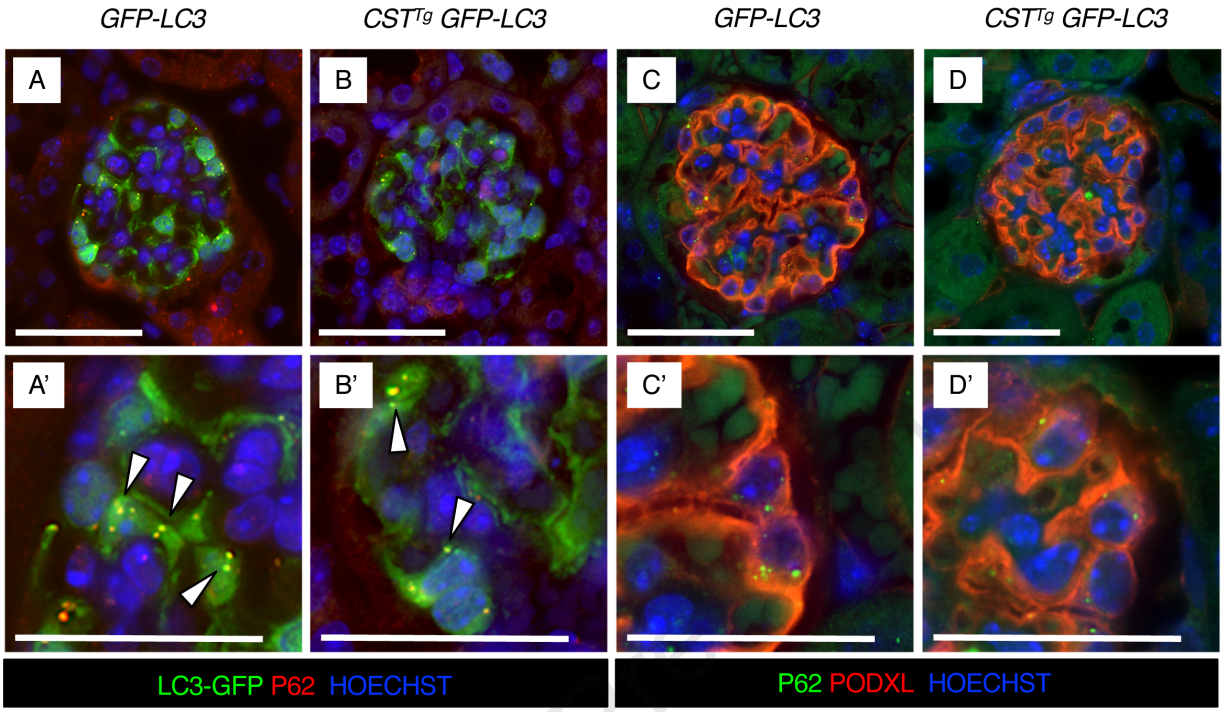
GFP-LC3
CSTTg GFP-LC3
GFP-LC3
CSTTg GFP-LC3
A
B
C
D
A'
B'
C'
D'
LC3-GFP P62 HOECHST
P62 PODXL HOECHST

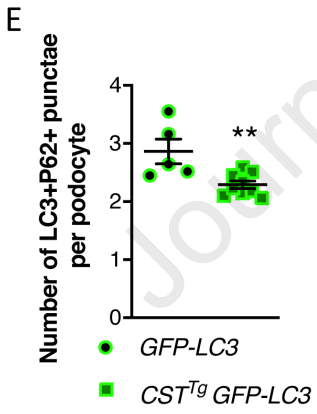
E
Number of LC3+P62+ punctae per podocyte
4
3
2
1
0
**
GFP-LC3
CSTTg GFP-LC3

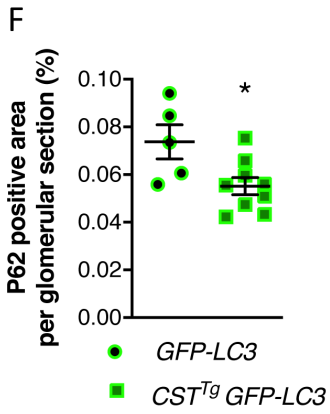
F
P62 positive area per glomerular section (%)
0.10
0.08
0.06
0.04
0.02
0.00
*
GFP-LC3
CSTTg GFP-LC3

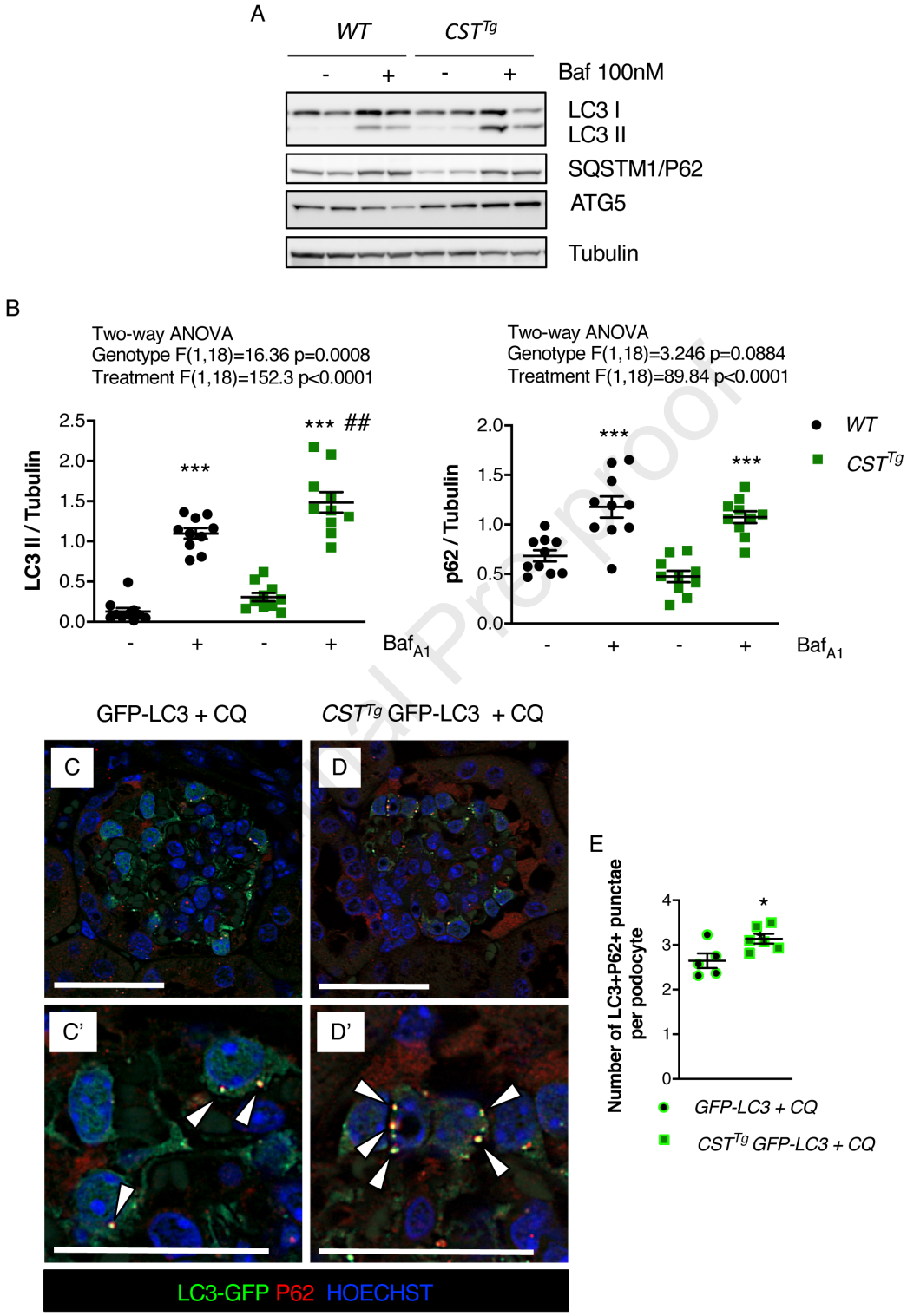
A
WT
CST^Tg
- + - +
Baf 100nM
LC3 I
LC3 II
SQSTM1/P62
ATG5
Tubulin
B
Two-way ANOVA
Genotype F(1,18)=16.36 p=0.0008
Treatment F(1,18)=152.3 p<0.0001
LC3 II / Tubulin
*** *** ##
Baf A1
Two-way ANOVA
Genotype F(1,18)=3.246 p=0.0884
Treatment F(1,18)=89.84 p<0.0001
p62 / Tubulin
*** ***
Baf A1
WT
CST^Tg
GFP-LC3 + CQ
CST^Tg GFP-LC3 + CQ
C
D
C'
D'
LC3-GFP P62 HOECHST
E
Number of LC3+P62+ punctae per podocyte
*
GFP-LC3 + CQ
CST^Tg GFP-LC3 + CQ

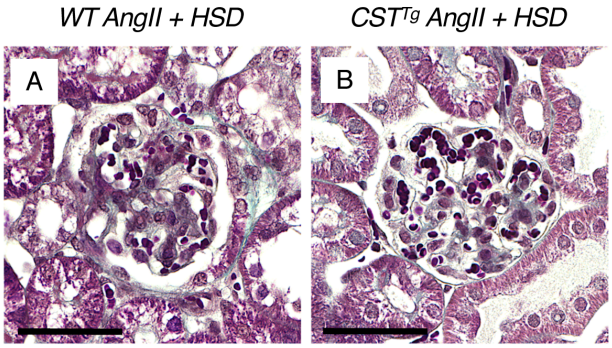
WT AngII + HSD
CSTTg AngII + HSD
A
B

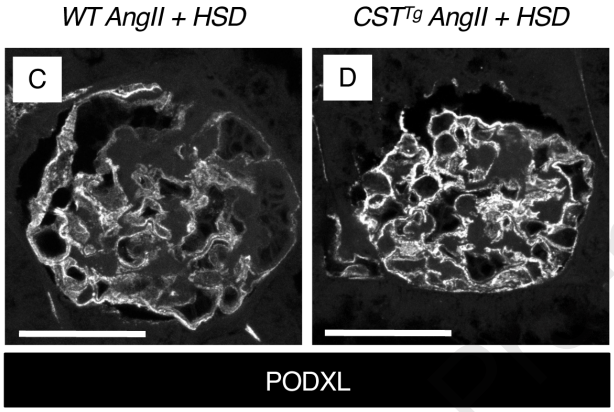
WT AngII + HSD
CSTTg AngII + HSD
C
D
PODXL

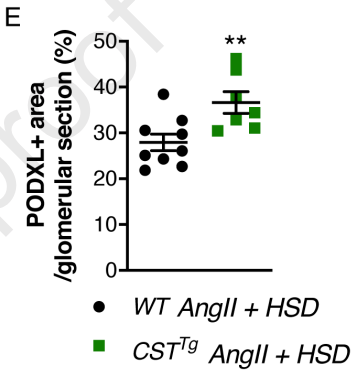
E
PODXL+ area /glomerular section (%)
50
40
30
20
10
0
**
WT AngII + HSD
CSTTg AngII + HSD

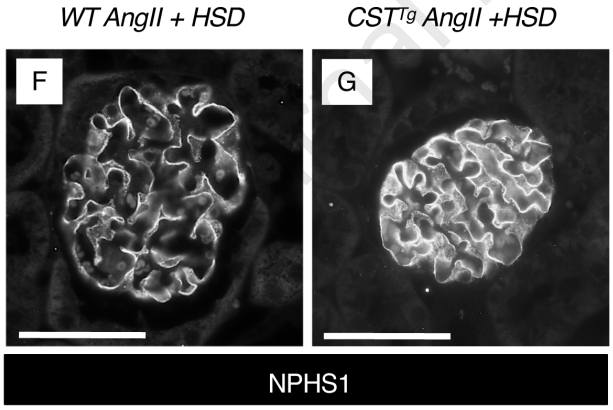
WT AngII + HSD
CSTTg AngII +HSD
F
G
NPHS1

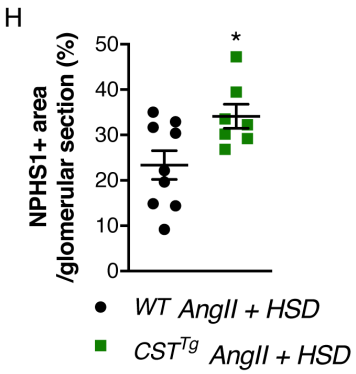
H
NPHS1+ area /glomerular section (%)
50
40
30
20
10
0
*
WT AngII + HSD
CSTTg AngII + HSD

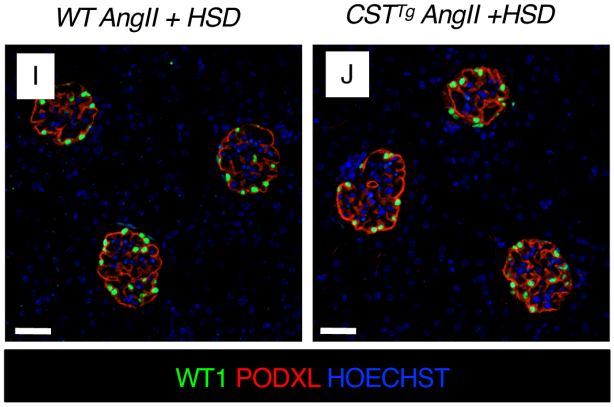
WT AngII + HSD
CSTTg AngII +HSD
I
J
WT1 PODXL HOECHST

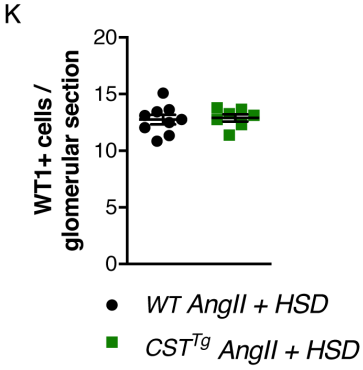
K
WT1+ cells / glomerular section
20
15
10
5
0
WT AngII + HSD
CSTTg AngII + HSD

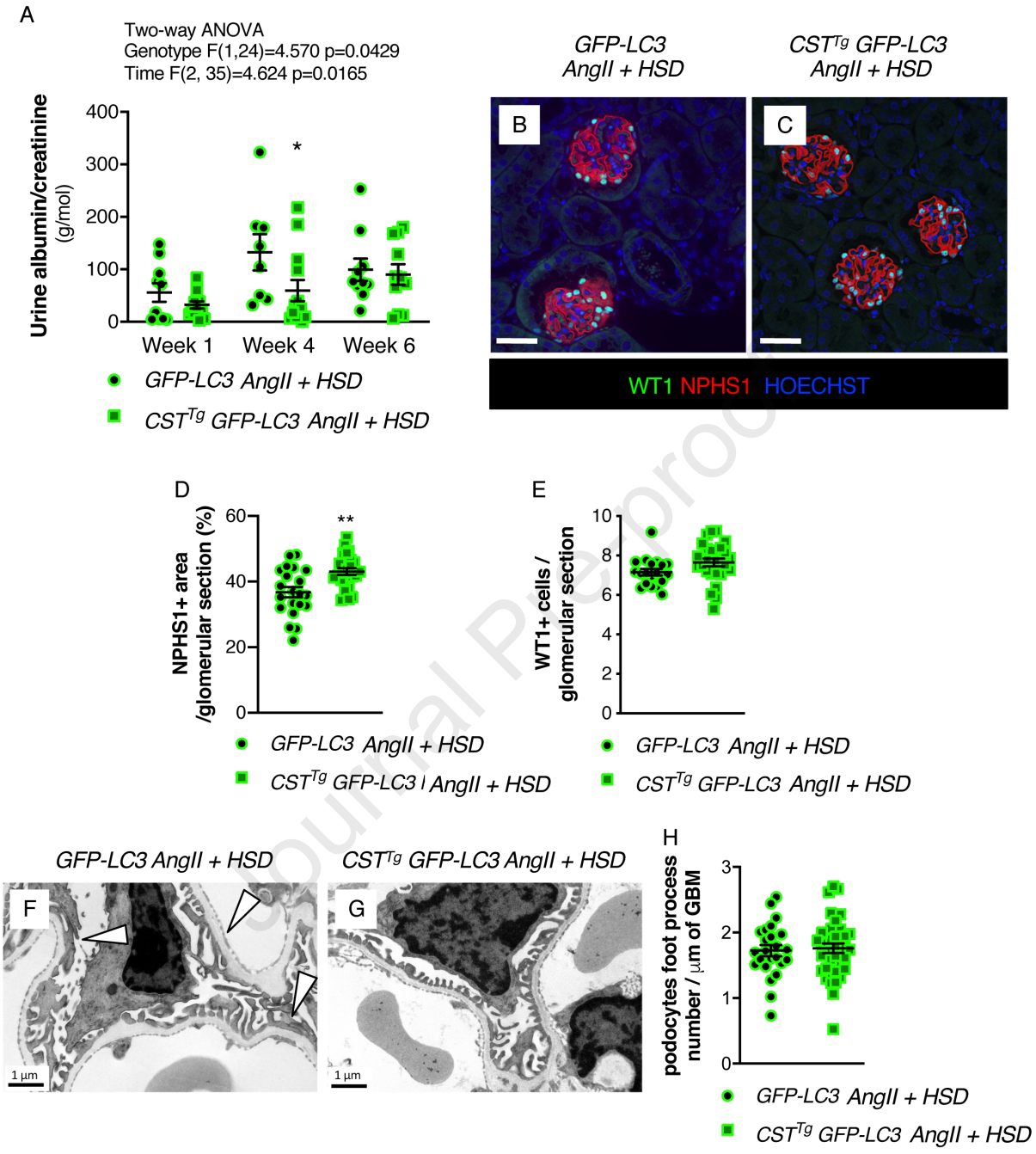
A
Two-way ANOVA
Genotype F(1,24)=4.570 p=0.0429
Time F(2, 35)=4.624 p=0.0165
Urine albumin/creatinine (g/mol)
400
300
200
100
0
*
Week 1
Week 4
Week 6
GFP-LC3 AngII + HSD
CSTTg GFP-LC3 AngII + HSD
GFP-LC3 AngII + HSD
CSTTg GFP-LC3 AngII + HSD
B
C
WT1 NPHS1 HOECHST
D
NPHS1+ area /glomerular section (%)
60
40
20
0
**
GFP-LC3 AngII + HSD
CSTTg GFP-LC3 AngII + HSD
E
WT1+ cells / glomerular section
10
8
6
4
2
0
GFP-LC3 AngII + HSD
CSTTg GFP-LC3 AngII + HSD
GFP-LC3 AngII + HSD
CSTTg GFP-LC3 AngII + HSD
F
G
1 µm
1 µm
H
podocytes foot process number / µm of GBM
3
2
1
0
GFP-LC3 AngII + HSD
CSTTg GFP-LC3 AngII + HSD

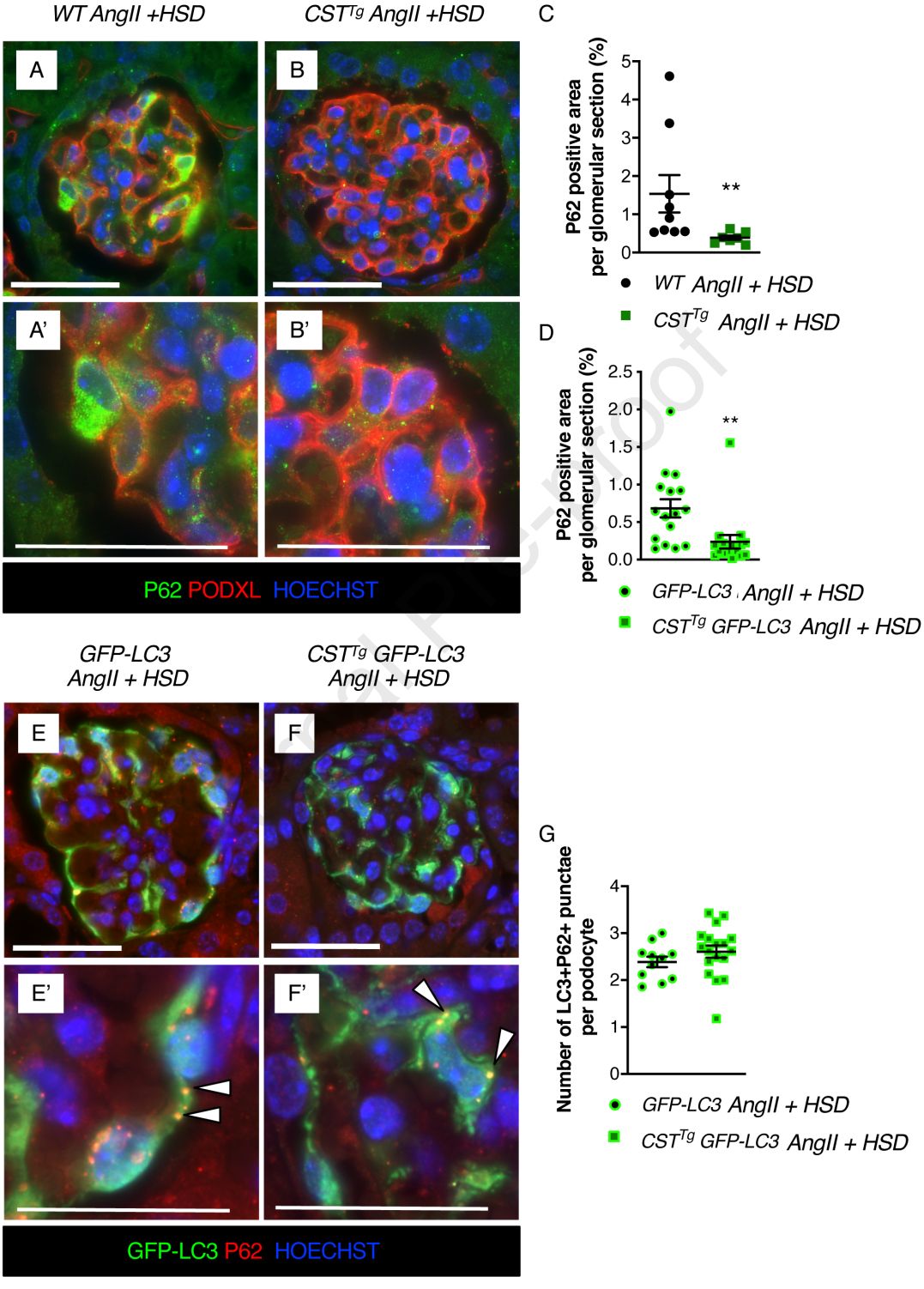
WT AngII +HSD
CSTTg AngII +HSD
A
B
A'
B'
P62 PODXL HOECHST
C
P62 positive area per glomerular section (%)
0
1
2
3
4
5
**
WT AngII + HSD
CSTTg AngII + HSD
D
P62 positive area per glomerular section (%)
0.0
0.5
1.0
1.5
2.0
2.5
**
GFP-LC3 AngII + HSD
CSTTg GFP-LC3 AngII + HSD
GFP-LC3 AngII + HSD
CSTTg GFP-LC3 AngII + HSD
E
F
E'
F'
GFP-LC3 P62 HOECHST
G
Number of LC3+P62+ punctae per podocyte
0
1
2
3
4
GFP-LC3 AngII + HSD
CSTTg GFP-LC3 AngII + HSD

A

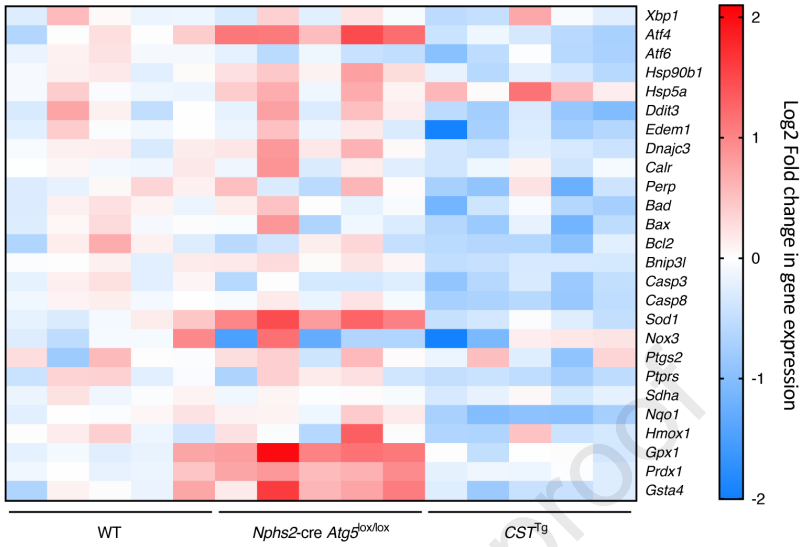

B

WT vs. Nphs2-cre Atg5$^{lox/lox}$	Log2 Fold change of gene expression	*P* value
Sod1	1,135	0,000414
Prdx1	0,751	0,000699
Atf4	1,118	0,001519
Atf6	-0,368	0,011152
Gpx1	1,286	0,013012
Hsp90b1	0,386	0,037785
Casp3	-0,304	0,04655

C

WT vs. CST^{Tg}	Log2 Fold change of gene expression	*P* value
Casp8	-0,676	0,000017
Nqo1	-0,877	0,00005
Bnip3l	-0,396	0,001458
Casp3	-0,614	0,002444
Dnajc3	-0,371	0,004811
Bax	-0,638	0,005067
Hsp90b1	-0,380	0,007758
Edem1	-0,776	0,008106
Atf6	-0,533	0,01096
Bad	-0,554	0,015655
Ptprs	-0,545	0,019105
Ddit3	-0,689	0,042243